2002

# Effect of tip geometry on blade tip flow and heat transfer

David Michael Kontrovitz
*Louisiana State University and Agricultural and Mechanical College*

# EFFECT OF TIP GEOMETRY ON BLADE TIP FLOW AND HEAT TRANSFER

**A Thesis**

**Submitted to the Graduate Faculty of the**
**Louisiana State University and**
**Agricultural and Mechanical College**
**in partial fulfillment of the**
**requirements for the degree of**
**Master of Science in Mechanical Engineering**

**in**

**The Department of Mechanical Engineering**

**by**
**David Michael Kontrovitz**
**B.S.M.E., Louisiana State University, 2000**
**August 2002**

# Acknowledgements

I would like to thank my advisor Dr. Srinath V. Ekkad. I am forever grateful for the wealth of knowledge he has imparted to me over the years. I deeply appreciate his guidance and advice, his limitless patience and good humor, and the encouragement he has given me. I also thank Dr. Ekkad for the financial support I received while at LSU.

I thank Dr. Sumanta Acharya and Dr. Dimitris E. Nikitopoulos for their help and advice, contributions to my education, and suggestions regarding this thesis. I also thank them for serving as members of my committee.

I am grateful to all of my colleagues past and present. I thank Hasan for his assistance with the ANSYS models in this thesis, assistance in the lab, and advice regarding course work. I also thank Gautam Pamula for his assistance in the lab, advice on course work, and for helping me learn to use the visual processing system. I would like to thank Dr. Huitao Yang for his assistance in setting up the experimental test rig.

This project was funded by a grant from the NSF. Thanks to GE and Ron Bunker for the information they provided. Finally, I thank my entire family and all of my friends. Thanks to my parents for their constant support and the guidance they have given my throughout my life. Thanks to my sister for all of her encouragement. You are all truly appreciated.

# Table of Contents

# List of Tables

# List of Figures

# Nomenclature

| | |
|---|---|
| C | Chord |
| D | squealer depth |
| h | Convective heat transfer coefficient |
| k | thermal conductivity of Plexiglas test surface |
| H | height of test blade |
| M | Mach number |
| P | pressure |
| PR | pressure ratio |
| Re | free stream Reynolds number, $\rho VC/\mu$ |
| S | blade spacing |
| t | time of color change |
| T | temperature |
| Tu | free stream turbulence |
| V | free stream velocity |
| x | distance |

Greek Symbols

| | |
|---|---|
| $\alpha$ | thermal diffusivity of Plexiglas test surface |
| $\rho$ | density of air |
| $\mu$ | viscosity of air |

Subscripts

| | |
|---|---|
| e | exit |

| | |
|---|---|
| i | initial condition, inlet |
| m | bulk flow or mainstream |
| o | total |
| r | liquid crystal color red |
| s | static |

# Abstract

In an attempt to increase thrust to weight ratio and efficiency of modern gas turbines, engine designers are always interested in increasing turbine operating temperatures. The benefits are attributed to the fact that higher temperature gases yield a higher energy potential. However, the detrimental effects on the components along the hot gas path can offset the benefits of increasing the operating temperature. The High Pressure Turbine (HPT) first stage blade is one component that is extremely vulnerable to the hot gas. The present study explores the effects of gap height and tip geometry on heat transfer distribution. This investigation differs from those in the past because the tip profile from an in-service High Pressure Turbine of an aircraft engine was used. Other experiments have used the $E^3$ test blade or a power generation blade that have different characteristics. The pressure ratio (inlet total pressure to exit static pressure) used was 1.2 which is lower than the actual pressure ratio this blade sees in service (PR = 1.7). A transient liquid crystal technique was used to obtain the tip heat transfer distributions similar to that used by Azad et al. (2000). Pressure measurements were made on the blade surface and on the shroud for different tip geometries and tip gaps to characterize the leakage flow and understand the heat transfer distributions.

# 1. Introduction

In an attempt to increase thrust to weight ratio and efficiency of modern gas turbines, engine designers are always interested in increasing turbine operating temperatures. The benefits are attributed to the fact that higher temperature gases yield a higher energy potential. However, the detrimental effects on the components along the hot gas path can offset the benefits of increasing the operating temperature. The High Pressure Turbine (HPT) first stage blade is one component that is extremely vulnerable to the hot gas.

Turbine blades convert energy from the combustor exhaust gases into mechanical energy. The mechanical energy is used drive the compressor, provided additional energy to aircraft systems, or in the case of a power generation gas turbine it is used to drive the generator. Although the entire blade is exposed to combustion gases, the blade tip region is most susceptible to oxidation and is usually found to be the first area to fail. According to Yang and Diller (1995), the pressure side tip corner from midchord to trailing edge is the most life limiting location. Figure 1.1 shows the region of the tip prone to failure.

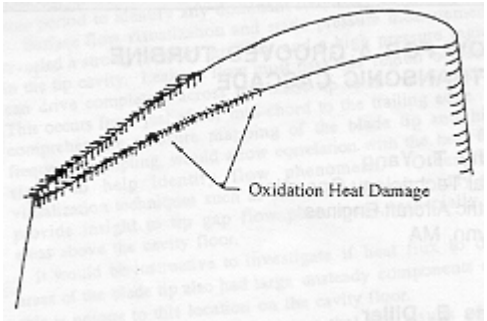


Figure 1.1: Leakage flow detrimental effects,Yang and Diller (1995)

The cause for tip failures are fairly well understood and can be explained as follows. A clearance gap between the rotating blade tip and stationary shroud is necessary to allow for the blade's mechanical and thermal growth during operation. Unfortunately, the gap allows for leakage flow from the pressure side to the suction side of the blade surface. The gas accelerates as it passes through the small gap. This leads to enhanced heat load to the blade tip region. Leakage flow, or clearance flow, also leads to undesirable aerodynamic losses not unlike the losses associated with airplane wing tips. In fact, one third of the losses through the turbine section can be attributed to leakage flow.

The effects of leakage flow are reduction in durability, blade life, and aerodynamic performance. At these elevated temperatures, the turbine blades are at risk of undergoing oxidation, spallation, thermal fatigue, and creep. The end result could be catastrophic failure.

## 1.1 Literature Survey

Bindon (1989) studied tip clearance loss, using a linear cascade, and concluded that the losses varied linearly with gap size. Bindon separated the total tip clearance loss into three components, and remarked that each loss component made different contributions to the total loss: internal gap loss 39%, suction corner mixing loss 48%, endwall/secondary loss 13%. Using static pressure measurements and flow visualization, Bindon observed a separation bubble on the blade suction edge that mixes with a high-speed leakage jet induced at midchord as shown in Figure 1.2. However, Bindon presented results in an atmospheric linear cascade. The leakage flow was not pressure

driven and this created a different type of leakage vortex than what would occur on an in-service blade tip.

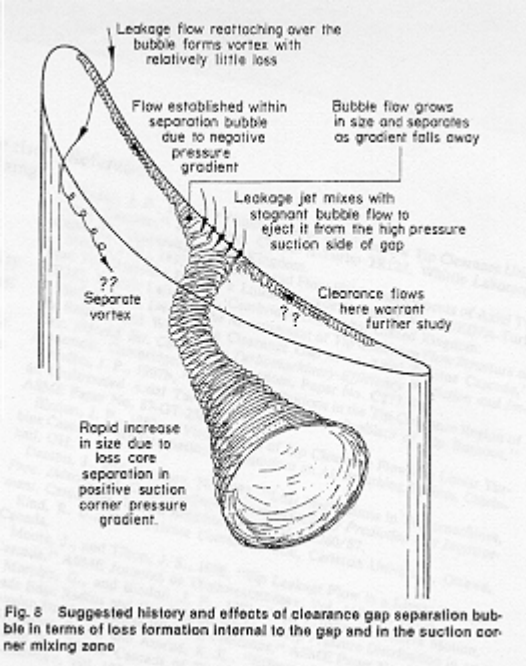


Figure 1.2: Leakage flow characteristics, Bindon (1989)

Yaras et al. (1989) also observed the presence of a separation bubble away from the leading edge and concluded that flow towards the leading edge had little effect on overall losses. In Yaras' study, a high-speed test rig was used. Consequently, the location of the separation bubble was farther back from the leading edge than Bindon (1989) reported. Yamamoto et al. (1989) also found that leakage vortices were sensitive to incident angle and the blade tip gap height.

One of the earliest heat transfer studies on turbine blade tip models by Mayle and Metzger (1982) established that the effects of relative motion between a blade model and the shroud have negligible effects on heat transfer data. They observed a small boundary

layer region that formed on the shroud. This important study allowed other researchers to model the blade with a stationary outer shell. Later, a blade model was used with a grooved top by Metzger et al. (1985) to investigate the effects of varying the recess depth. It was determined that tip heat transfer was reduced under the presence of a cavity. The cavity simulated a squealer tip geometry. Leakage flow was reduced until the depth reached D/W = 0.2. Metzger et al. (1985) also commented on the fact that there was an increase in heat transfer on the blade tip model's trailing edge.

A two-part study was conducted in 1988 using a water tunnel to model tip leakage as a sink flow (pressure side) and source flow (suction side). Part one, by Metzger and Rued (1988) looked at sink flow effects on the pressure surface. Metzger and Rued (1988) reported accelerated flow near the gap and relaminarization of the turbulent boundary layer. This resulted in a region of high heat transfer varing from two to ten gap widths. Part two, by Rued and Metzger (1988) dealt with source flow effects on the suction side. This experiment showed that the effects on the suction side heat transfer were greater (higher enhancement) and more complex as the leakage flow vortex is present on the suction side of the blade.

Moore et al. (1989) investigated the effects of Reynolds number in the tip gap region. This study included calculations for laminar flow conditions (Re: 100 – 10000) and both calculations and experimental results for turbulent flow. They managed to match turbulent and laminar calculations with experimental results. The conclusions were that the peak heat transfer was 1.85 times the fully developed downstream value for flow through parallel plates.

Metzger et al. (1990) used several heat flux gages on a blade tip model and compared the results to numerical calculations, and they found good agreement between the two. Yang and Diller (1995) were the first to perform an experiment on a realistic blade tip model, with a recessed tip, in a cascade wind tunnel. They reported that convective heat transfer coefficients were not dependent on tip gap height or local Mach number, however the conclusions were based on data taken with a single heat flux gage on the tip.

Bunker et al. (1999) published the first study with detailed blade tip heat transfer measurements. The measurements were made for a first stage power generation blade using a steady state liquid crystal technique. Bunker et al. (1999) varied the curvature of the blade tip edges (rounded and sharp). The blades were exposed to a pressure ratio of 1.45 and had a total turning ratio of 110 degrees. They found that the blade with a tip edge radius had greater leakage flow and higher heat transfer coefficients. Bunker et al. (1999) also reported that an increase in free stream turbulence intensity increased the heat transfer coefficient. The authors observed an area of low heat transfer toward the blade leading edge, referred to as the sweet spot.

Ameri and Bunker (1999) used CFD simulations to reproduce the results for the same blade geometry discussed in the previous paragraph. They concluded that the assumption of periodic flow was invalid for tip heat transfer calculations because the entire passage had to be modeled. Ameri and Bunker (1999) also found that the tip region heat transfer could be represented with a cell center finite volume scheme and a k-$\omega$ low Reynolds number turbulence model. Their numerical results for the radiused edge showed better agreement with the experimental data than that of the sharp edge. Figure

1.3 presents the numerical results from Ameri and Bunker (1999) for a radiused blade tip edge.

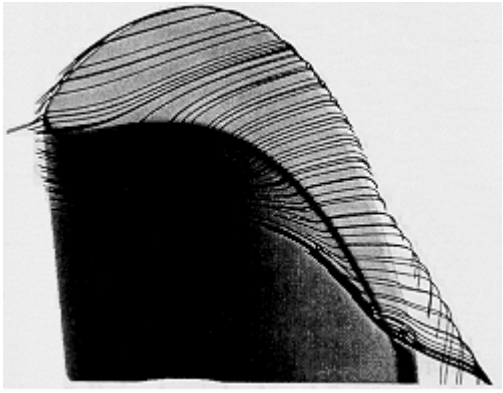

Figure 1.3: Simulated leakage flow pathlines, Ameri and Bunker (1999)

Recently, Azad et al. (2000) performed an experiment in which three different clearance gaps (C/H=1, 1.5, 2.5%) were used. They used a $E^3$ engine blade and a pressure ratio of 1.2 in a five blade cascade. They measured heat transfer coefficients using the transient liquid crystal technique. The results of this experiment showed that a larger gap causes higher heat transfer to the tip. A second study by Azad et al. investigated the effects of a recessed tip (D/H=3.77%) on the heat transfer coefficient. It was determined that the squealer tip produced a lower overall heat transfer coefficient compared to the plain tip. The squealer redirected the airflow over the tip forcing to move from the leading edge pressure side to the trailing edge suction side. It produced a different heat transfer patterns than that seen on a plain tip.

Bunker and Bailey (2000) investigated the effectiveness of chordwise sealing strips to reduce leakage flow and heat transfer. Sealing strips increased resistance to leakage flow. Sealing strips also reduced flow when the gap between the strip and shroud

was the same as that between the plain tip and shroud. The strip location affected the tip heat load distribution. Bunker and Bailey (2000) continued the study with more complicated strip geometries: circumferential rub strips, 45° angled rub strips. The experiments showed that circumferential and angled strips increase heat loads by 20 – 25% and 10 – 15% respectively.

The most recent study on squealer tips, by Bunker and Bailey (2001) looks at the relationship between squealer depth for a high-pressure turbine blade. The blade had a turning angle of 100 degrees, a pressure ratio of 1.41, clearance-to-cavity ratios of 0.67 and 2, and squealer depths 1.02, 1.78, 2.54, and 3.05mm. They found that a deeper tip cavity results in reduced heat transfer to the tip, although the distribution is non-uniform.

Azad et al. (2001) examined the benefits of six different squealers, including single and double squealers. The single squealer was a thin extension (2.3 mm) running from tip to tail, located on the chord, pressure edge or suction edge. The double squealer consists of two strips: a full perimeter strip, a pressure side strip from tip to tail and a short chord strip, and a suction side strip from tip to tail and a short chord strip. The single squealer produced lower heat transfer coefficients on the tip than the double squealers. The midchord squealer produced the best leakage reduction.

## 1.2 Present Study

Many parameters affect blade tip heat transfer. The total blade turning angle and general blade geometry, such as thickness, the presence of a squealer and edge radius, make a large contribution to the heat load distribution. Inlet Reynolds number and turbulence intensity can also affect the magnitude of the heat transfer coefficient. Over the years, researchers have found that tip gap height and squealer depth has a tremendous

influence on blade tip heat transfer. The effects of these parameters continue to be of interest to those working in the gas turbine industry.

The present study explores the effects of gap height and tip geometry on heat transfer distribution. This investigation differs from those in the past because the tip profile from an in-service High Pressure Turbine of an aircraft engine was used. Other experiments have used the $E^3$ test blade or a power generation blade that have different characteristics. The pressure ratio (inlet total pressure to exit static pressure) used was 1.2 which is lower than the actual pressure ratio this blade sees in service (PR = 1.7). A transient liquid crystal technique was used to obtain the tip heat transfer distributions similar to that used by Azad et al. (2000). Pressure measurements were made on the blade surface and on the shroud for different tip geometries and tip gaps to characterize the leakage flow and understand the heat transfer distributions.

# 2. Description of Test Facility

## 2.1 Wind Tunnel and Air Supply

This experiment uses a blow down test rig as illustrated in Figure 2.1. The test rig was designed to produce the required pressure ratio across the blade for a short duration.

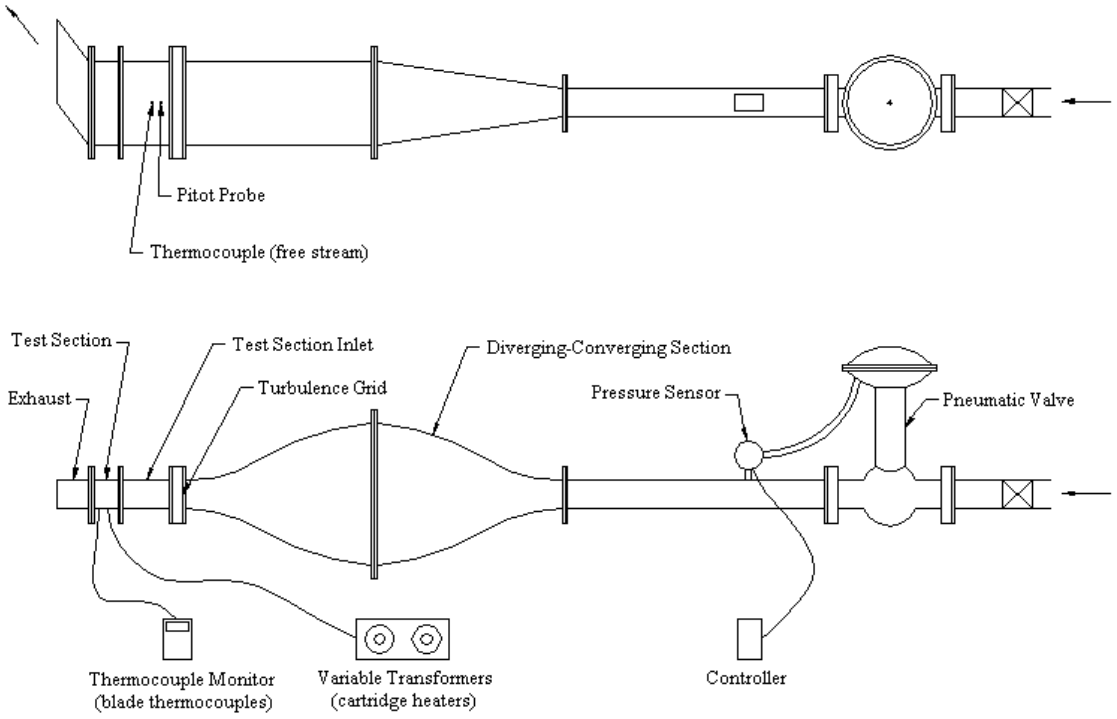


Figure 2.1: Experimental rig

An Atlas Copco GR110 compressor equipped with a Pneumatech Inc. air dryer supplies air to a large tank capable of holding 2000 gallons of high pressure air. This system is capable of generating a steady flowrate of 0.5 kg/s.

The test section is part of an open loop blowdown setup, which is shown in Figure 2.1. Air first passes through a gate valve. The gate valve allows the entire wind tunnel to be isolated from the supply tank. Downstream from that valve is a large pneumatically actuated Fisher control valve, which is shown in Figure 2.2. A Fisher-Rosemount DPR 960 controller regulates the pneumatic valve. The controller allows one to set the valve and maintain a specified valve opening and/or operating pressure in the test section.

Figure 2.2: Pneumatic valve

Air then passes through a rectangular diverging-converging section. This section is placed directly upstream from the test section. Its purpose is to settle the flow and

make it more uniform before entering the test section. Boundary layer bleeds (slotted openings) along the test section inlet ensure the formation of a new boundary layer before the air enters the four-blade linear cascade test section.

The final major component is the cascade exhaust. The exhaust area is fitted with two tailboards. One tailboard is aligned with the pressure blade trailing edge and the other is aligned with the heat transfer blade. The tailboards are important because they are made adjustable and enable the user to equalize pressure in the passages adjacent to each blade and ensure periodic flow in all passages.

## 2.2 Test Section

The test section is a linear cascade with four, two-dimensional blade tip models. Blade geometry is taken from the tip section of a General Electric HPT blade. Each blade is made of aluminum using an EDM machine, and they bolt to a steel base plate that can easily be removed from the test section. The blade spacing (S) 95.25 mm, and the axial chord (C) 60.02 mm. The two outer blades guide airflow around the inner blades. Inner blades are used for pressure and heat transfer measurements. All blades have a length from root to tip (H) of 76.2 mm. Figure 2.3 shows the four-blade linear cascade.

Pressure measurements are made on the blade surface in order to map the surface distribution and ensure that the flow conditions during heat transfer tests are correct. The "pressure blade" (Figures 2.3, 2.4) outer surface is lined with small tubes, extending from root to tip, that are set in recesses. The blade is then covered by a thin, strong tape to make its surface smooth. Small holes are put in the tubes at the following locations for the purpose of making static pressure measurements: 33.3, 86.7, 100% of the span from

hub to tip (one hole per tube). Each alternate hole has a different spanwise location. Atotal of 96 taps are distributed among the three span locations.

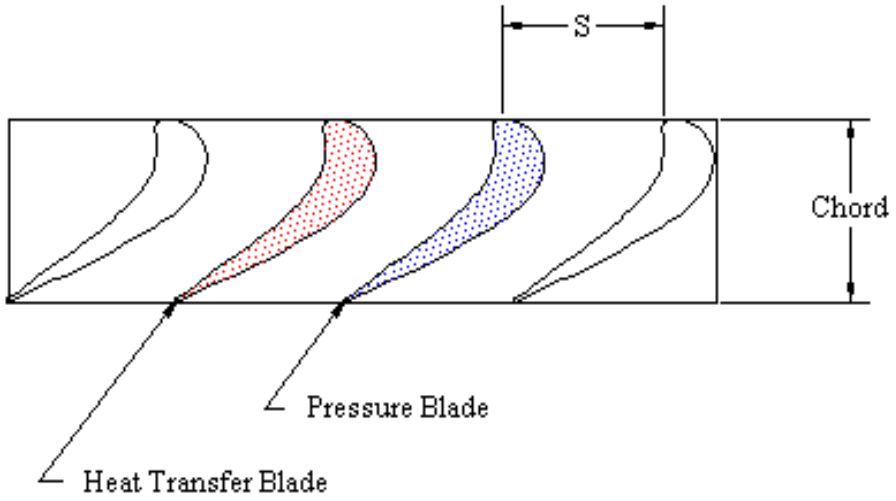


Figure 2.3: Test section schematic

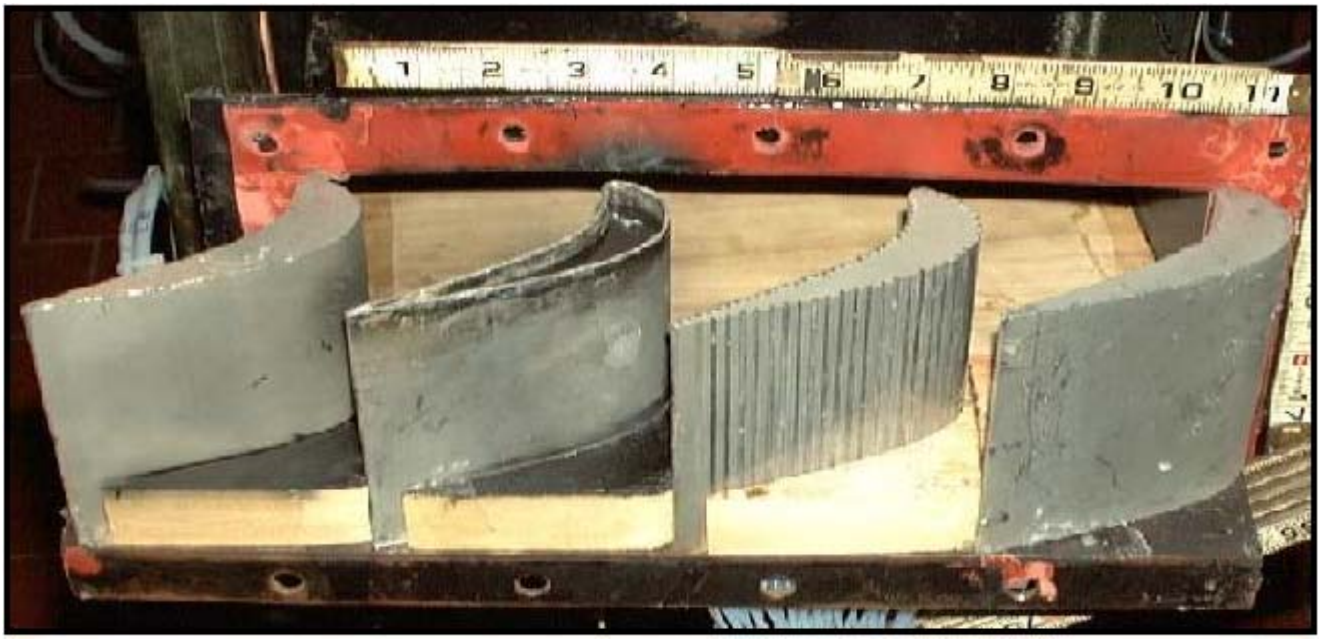

Figure 2.4: Test section photograph

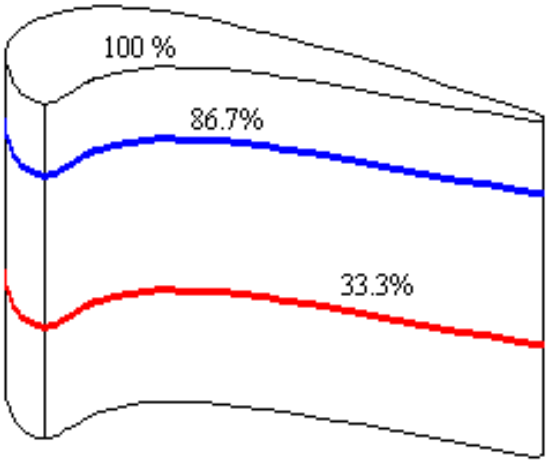


Figure 2.5: Pressure blade

Pressure measurements are also made on the shroud for each of the squealer tips and the flat tip cases as indicated in Figure 2.6. A special top plate with holes 6.35 mm away from the suction side, 6.35 mm from the pressure side, and along the chamber line, allows pressure measurements on the stationary shroud.

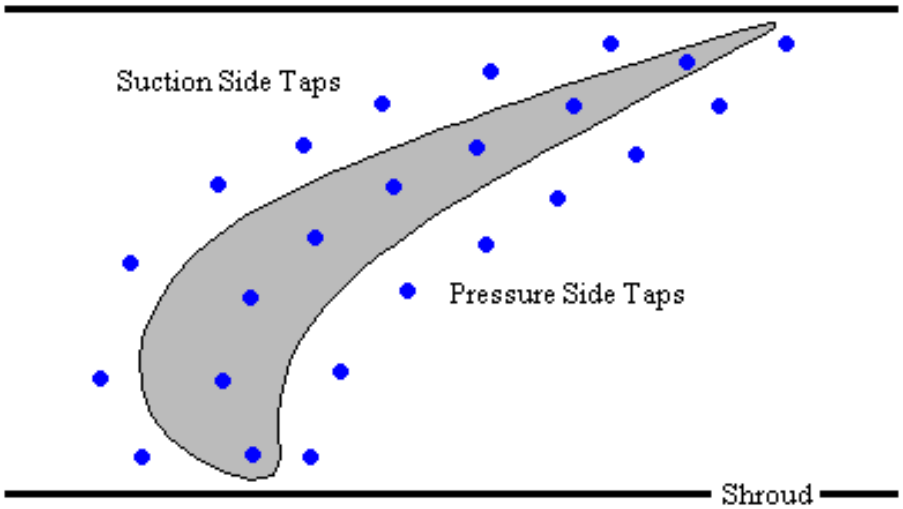


Figure 2.6: Shroud pressure taps over heat transfer blade

The photograph in Figure 2.7 presents the Pressure Systems, NetScanner, Model 98RK which is used for all pressure measurements.

Figure 2.7: Net Scanner

A “heat transfer blade” allows heat transfer measurements (Figure 2.3, 2.4, 2.8). A 25.4 mm recess is in the top of this blade; various Plexiglas inserts fit into the recess and allow for variable groove depth. Two depths are made with the inserts: D = 3.175, 6.35 mm. The squealer rim, left after machining the recess, is 1.5875 mm thick.

A Hallcrest Liquid Crystal sheet (R25C5W 25-30°C) is on each Plexiglas insert. The sheet changes color, from red to green, as the blade cools (see Procedures). Color change occurs at 26.3 °C. A special Plexiglas top plate is used during the heat transfer

experiments so that the image processing equipment can “see” the blade tip and record the color change.

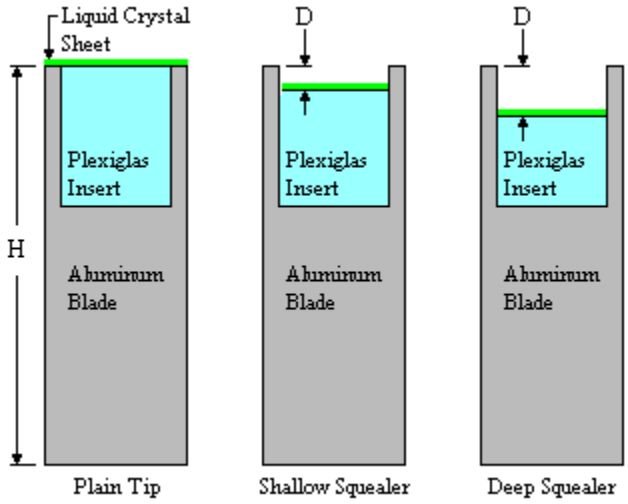


Figure 2.8: Heat transfer blade

The experimental procedures involve heating the heat transfer blade to a high temperature then cooling it with compressed air in a blowdown mode. Two Hotwatt cartridge heaters are imbedded in the blade aluminum core to heat the blade. These heaters have a length and diameter of 31 mm and 6.35 mm respectively. The cartridge heaters have stainless steel sheaths and are capable of reaching temperatures up to 676°C, however they are never operated above 110 °C during testing.

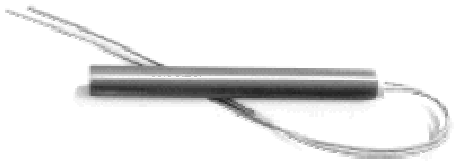

Figure 2.9: Hotwatt cartridge heater

Each heater connects to a Staco Variable Autotransformer (Figure 2.10), which allows the user to adjust the amount of current going into each heater and thereby controlling the blade temperature. A type-k thermocouple is between the Plexiglas insert and the aluminum blade, and additional thermocouples are on the blade tip. The thermocouples are monitored to ensure that a uniform blade temperature is maintained.

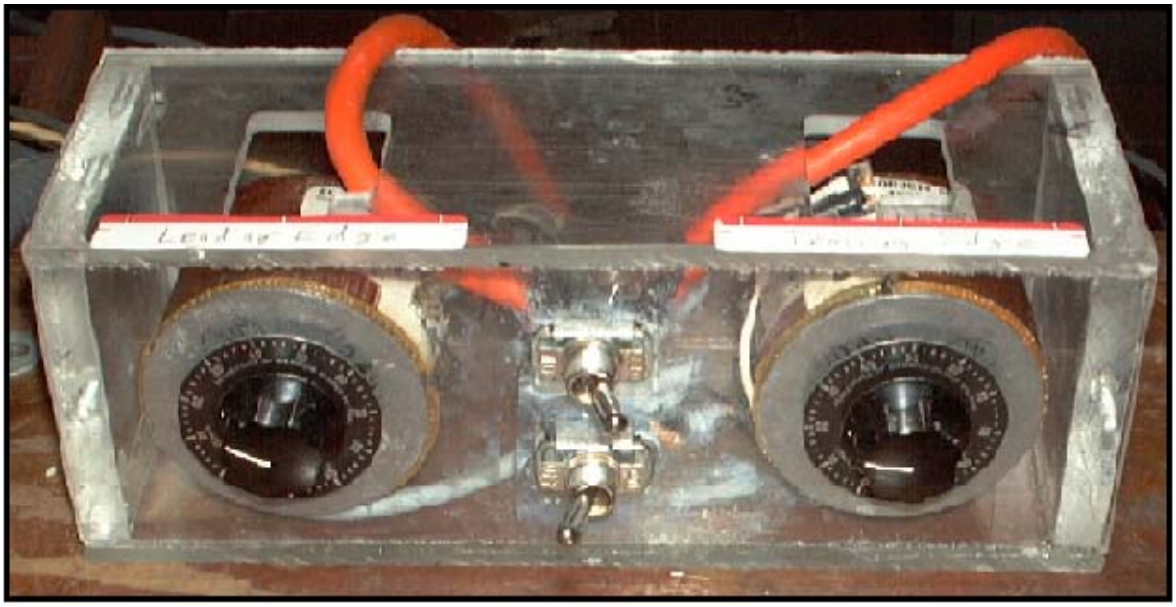

Figure 2.10: Variable transformers

## 2.3 Visual Processing System

Figure 2.11 gives a schematic of the image processing system used for this study. A Plunix RGB camera (Figure 2.12) records the liquid crystal color change on the heat transfer blade.

This camera, which is directly over the blade tip, connects to a CFG 24-bit frame grabber board in a PC. Image processing software (Optimas v6.5) communicates with the frame grabber board. A macro allows Optimas to record the time at which the liquid

crystal changes from green to red. It produces a time file, which gives the time of change for each pixel to turn red i.e. 26.3 °C during the blowdown test.

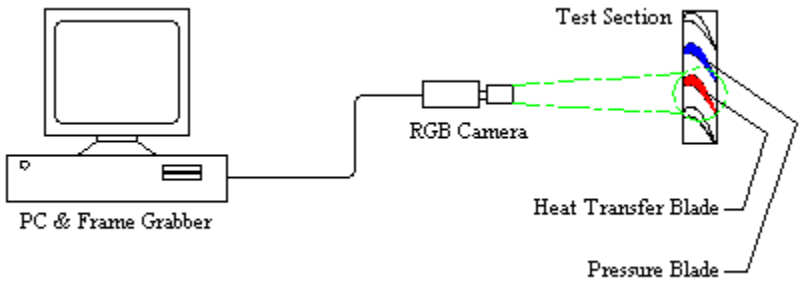


Figure 2.11: Visual processing system


Figure 2.12: Camera

# 3. Experimental Procedures

The two types of experiments in this study are the pressure tests and the heat transfer tests. The purpose of the pressure tests is to map the flow around the blade surface and on the shroud by obtaining static pressure measurements. The purpose of the heat transfer tests is to determine the blade tip heat transfer coefficients. The basic procedures for running these tests are similar.

## 3.1 Heat Transfer Test

The heat transfer blade is heated for two hours to ensure that its temperature reaches steady state before testing. During heating, thermocouples are used to monitor the blade internal and external temperature. These thermocouples are checked every 5-15 minutes.

Once the blade is at steady state, the camera is focused on the heat transfer blade tip. Lights are also focused on the test surface to illuminate the tip surface for color capture. A region of interest or ROI (a rectangular area surrounding the test surface) is selected using the image processing software Optimas. This region of interest is the same for all heat transfer tests. Background intensity is set to ensure that lighting is uniform. A threshold is set to indicate the onset of actual color change during the transient test.

The compressor is run and the supply tank is filled to 1,896,058 Pa (275 psig). Note that the same pressure is used for each experiment Although air leaves the tank, the short duration of test ensures that the tank never fully empties. The heaters are switched off, and the pneumatic valve is then opened so that air may enter the test rig. The

experiment ends when the entire surface area changes color to red. The experiment takes 30 – 60 seconds to complete.

## 3.2 Pressure Test

Static pressure measurements are made on the shroud for each blade tip configuration. Measurements are also made on the pressure blade suction and pressure surfaces. This aids in mapping the flow field around the blade to study leakage effects.

The pressure system is supplied with 861,844 Pa of pressure to drive internal valves. Before each pressure test, moisture is blown from the pressure system data ports using the supply pressure. The data ports are calibrated and reset to zero, when necessary, to ensure accuracy. Tubes connected to the blade or shroud are tightly plugged into the Pressure System data ports. Each tube is tested to ensure no leakage at the point of connection, and to make sure there are not tore or frayed. This is accomplished with a quick test in which the rig is filled with compressed air.

The compressor is run and the supply tank is filled to 1,896,058 Pa. Note that the same pressure is used for each experiment. Although air leaves the tank, the short duration of the test ensures that the tank never fully empties. The pneumatic valve is then opened and air enters the test rig. The duration of all pressure tests matched that of the heat transfer tests. The pressure system reads surface static pressures and outputs a large data file, which gives data in the form of an Excel spreadsheet.

# 4. Heat Transfer Theory

## 4.1 Semi-Infinite Solid Assumption

The theory for this study requires the assumption that the Plexiglas insert is a semi-infinite solid.

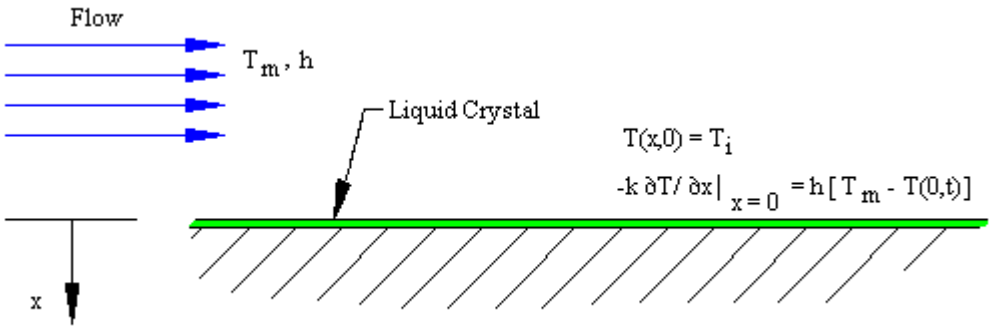


Figure 4.1: Semi-infinite solid

The semi-infinite solid assumption is valid for this test blade for two reasons. The duration of the experiment is small. It lasts for less than one minute. Secondly, Plexiglas has high thermal capacity. Therefore temperature penetration does not exceed wall thickness.

The equation for transient heat conduction through a semi-infinite solid wall is as follows:

$$\frac{\partial^2 T}{\partial x^2} = \frac{1}{\alpha}\frac{\partial T}{\partial t} \tag{4-1}$$

The boundary condition at x=0 is:

$$-k\frac{\partial T}{\partial x}|_{x=0}=h[T_m-T(0,t)] \tag{4-2}$$

The initial condition is:

$$T(x,0)=T_i \tag{4-3}$$

The following equation is derived from 4-1, 4-2, 4-3:

$$\frac{T_r-T_i}{T_m-T_i}=erfc\left(\frac{x}{2\sqrt{\alpha t}}\right)-\left[\exp\left(\frac{hx}{k}+\frac{h^2\alpha t}{k^2}\right)\right]\left[erfc\left(\frac{x}{2\sqrt{\alpha t}}+\frac{h\sqrt{\alpha t}}{k}\right)\right] \tag{4-4}$$

Heat transfer measurements are make on the blade surface region where x=0. Therefore equation 4-4 can be reduced:

$$\frac{T_r-T_i}{T_m-T_i}=1-\left[\exp\left(\frac{h^2\alpha t}{k^2}\right)\right]\left[erfc\left(\frac{h\sqrt{\alpha t}}{k}\right)\right] \tag{4-5}$$

In equations 4-5, $T_i$ is the initial temperature of the test blade. $T_i$ is the highest of the three temperatures in equation 4-5. $T_m$ is the mainstream static temperature, which is the lowest temperature. $T_r$ is the temperature at which liquid crystal becomes red, and its value is between mainstream and initial blade temperature. The variable t is the time at

which liquid crystal turns red. The constant k is Plexiglas thermal conductivity, which is low relative to other engineering materials. The constant α is Plexiglas thermal diffusivity, which is high relative to other engineering materials. Heat transfer coefficient, h, is the only unknown in equations 4-5.

## 4.2 Analysis of Semi-Infinite Solid Assumption

In order to verify the validity of the semi-infinite solid assumption, a two-dimensional transient analysis is performed with ANSYS software. Blade geometry is input for a location between the leading and trailing edges. The transient analysis lasts for thirty seconds, which corresponds to the average test duration. The finest mesh for this analysis contained 12,659 elements. Boundary conditions are as follows: heat transfer coefficients of 800, 1000, 1300 $W/m^2$ K on the tip, pressure side and suction side respectively, the free stream temperature is 288°K, and the initial blade temperature is 383°K. Graphs were obtained for three locations, which extend 12.7mm into the blade as illustrated Figure 4.2.

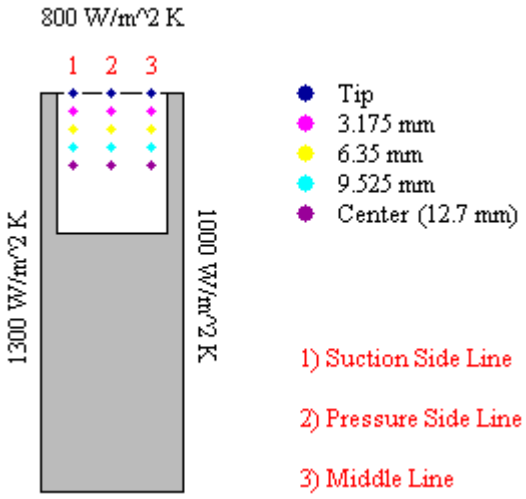


Figure 4.2: ANSYS blade

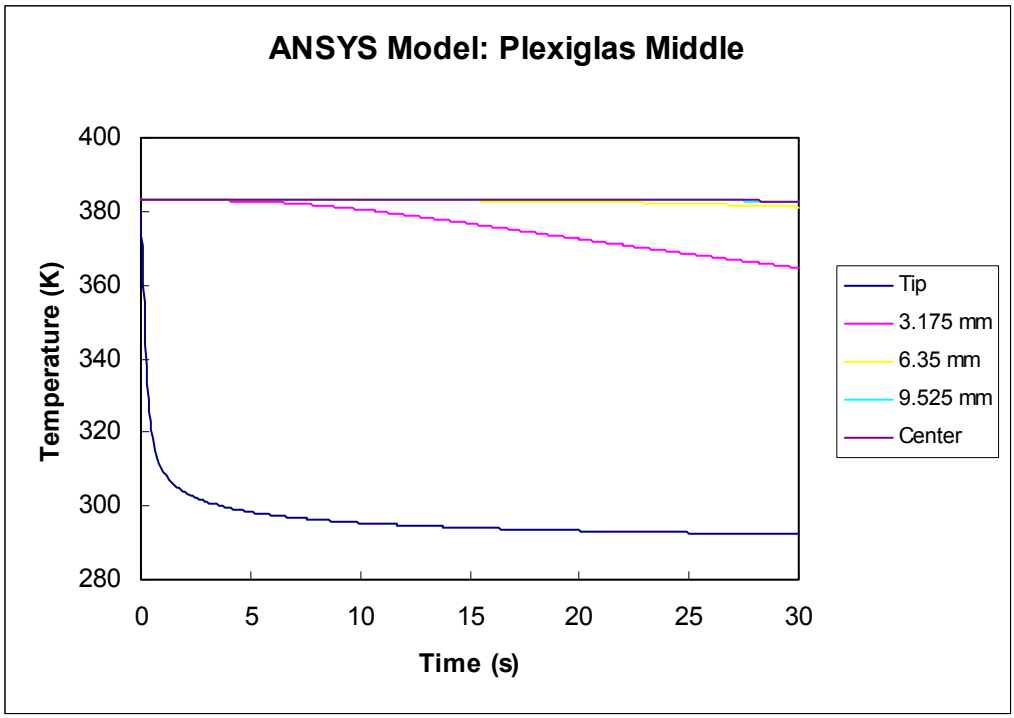


Figure 4.3: ANSYS model, Plexiglas middle

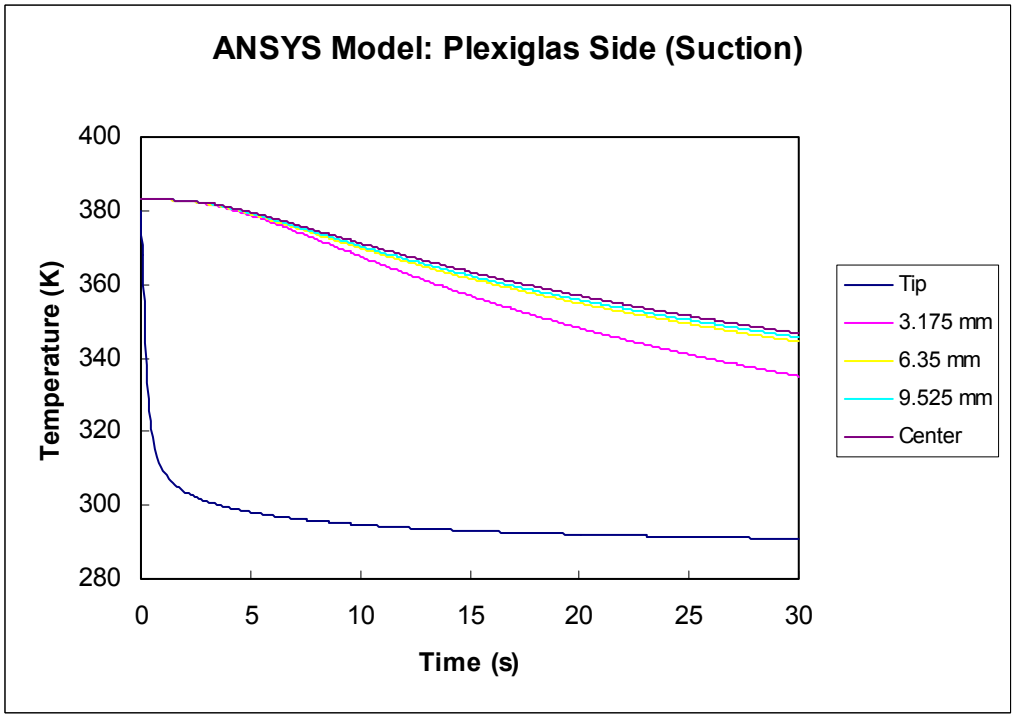


Figure 4.4: ANSYS model, Plexiglas side (suction)

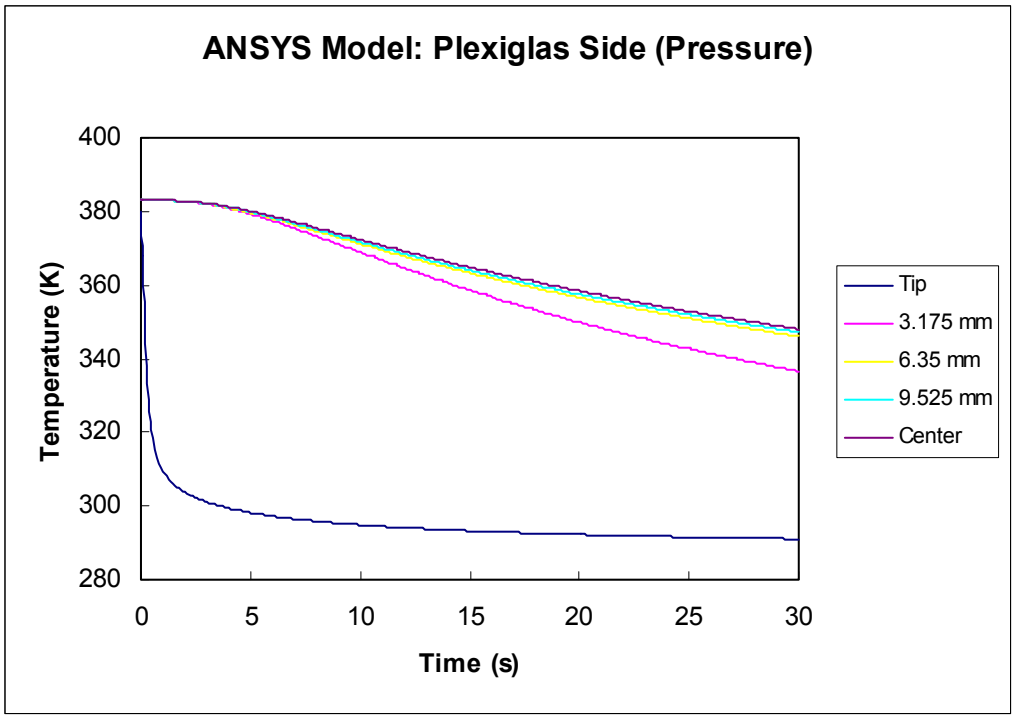


Figure 4.5: ANSYS model, Plexiglas side (pressure)

Figure 4.3 presents the temperature response in the Plexiglas middle region. The center temperature does not change drastically. The blade tip temperature does drop significantly. All other temperatures, at points between the tip and center, drop slightly. The temperature penetration into the Plexiglas test section is insignificant.

Figure 4.5 presents the temperature response in the Plexiglas near the suction side. The center temperature drops 20°K in 30 seconds due to high heat transfer coefficient on the suction side. Note that during a typical heat transfer test, color change over most of the blade tip occurs within the first five to twenty seconds, so the calculations in the high heat transfer regions are not as affected by temperature penetration. The blade tip temperature drops significantly. All other temperatures, at point between the center and tip, drop slightly more than the center temperature. The temperature penetration into the Plexiglas test section is insignificant.

Figure 4.4 presents the temperature response in the Plexiglas near the suction side. Results in Figure 4.4 are similar to those in Figure 4.5, but the temperature drop is slightly lower.

# 5. Cascade Flow Characterization

## 5.1 Blade Passage Equalization

Before running any experiments, it is necessary to equalize flow through the three passages. Equalizing the passages ensures that the flow field around the pressure and heat transfer blades is identical. Small holes are located on the shroud at identical locations above each passage. Figure 5.2 shows local $P_s/P_o$ values after equalization.

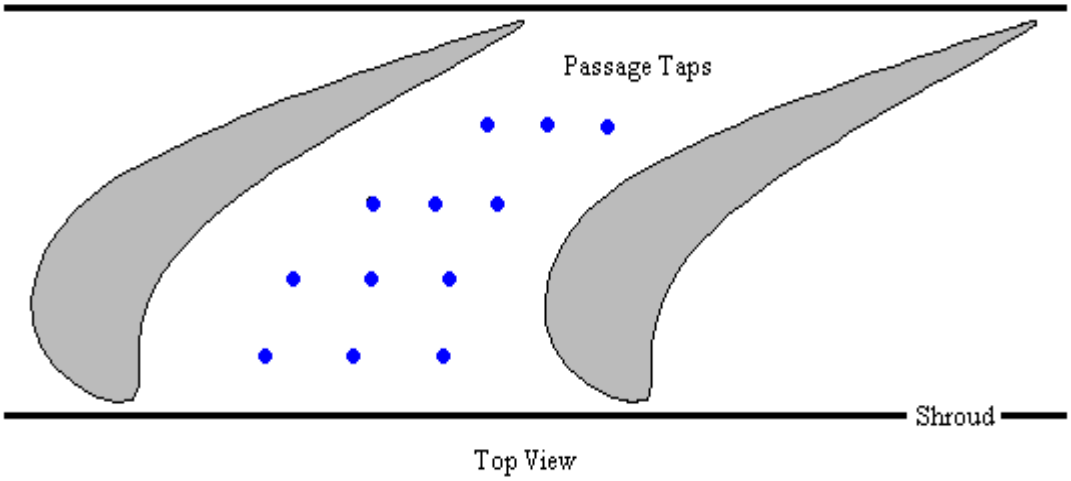


Figure 5.1: Shroud pressure taps over passages

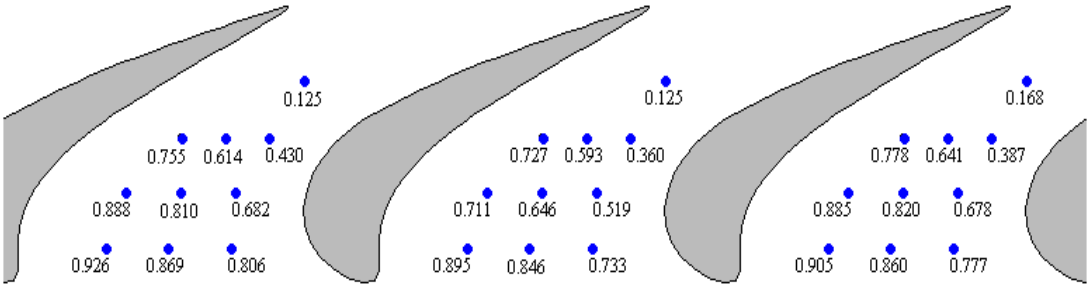


Figure 5.2: Equalized passage pressure distributions

## 5.2 Pressure Drop

During a blow-down test the supply tank, which provides air to the test rig, empties into the test section. Therefore the inlet total pressure does not remain constant. A test was preformed to determine the total pressure variation during the blowdown operation. Inlet total pressure is measured with a pitot probe (located 23 cm upstream of the test blades at midspan) and the NetScanner system.

The following graph presents pressure drop by relating the inlet total pressure to time. Note the fact that the majority of the liquid crystal color change takes place within the first five to ten seconds of the heat transfer test. The total pressure peaks immediately after the valve opens and then drops steadily for the duration of the test. The variation during the test from highest to lowest is 3-5%.

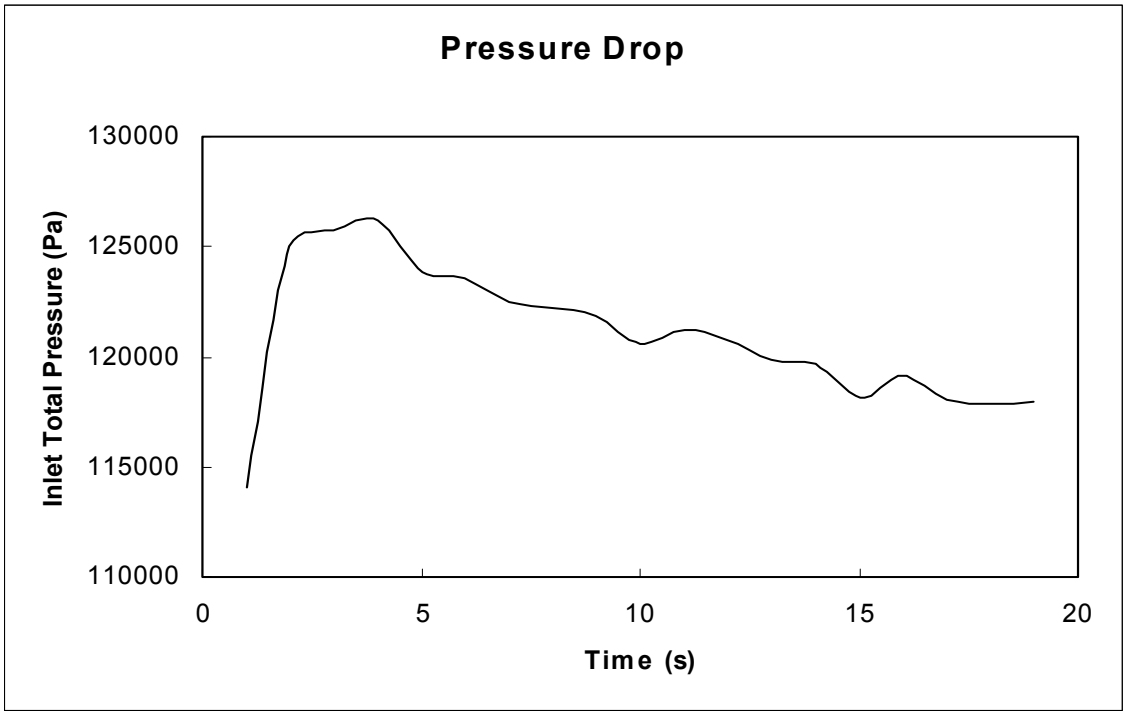


Figure 5.3: Pressure drop during the blowdown test

## 5.3 Blade Surface Pressure Distribution

Local static pressure measurements ($P_s/P_o$) on the pressure blade are presented in Figure 5.4. The measurements are for the blade pressure side, referred to as (a), and the suction side, referred to as (b). Pressure distributions are plotted for three different span locations. The locations from hub to tip are 33.3, 86.7, and 100% of the span, as explained in Chapter 2.

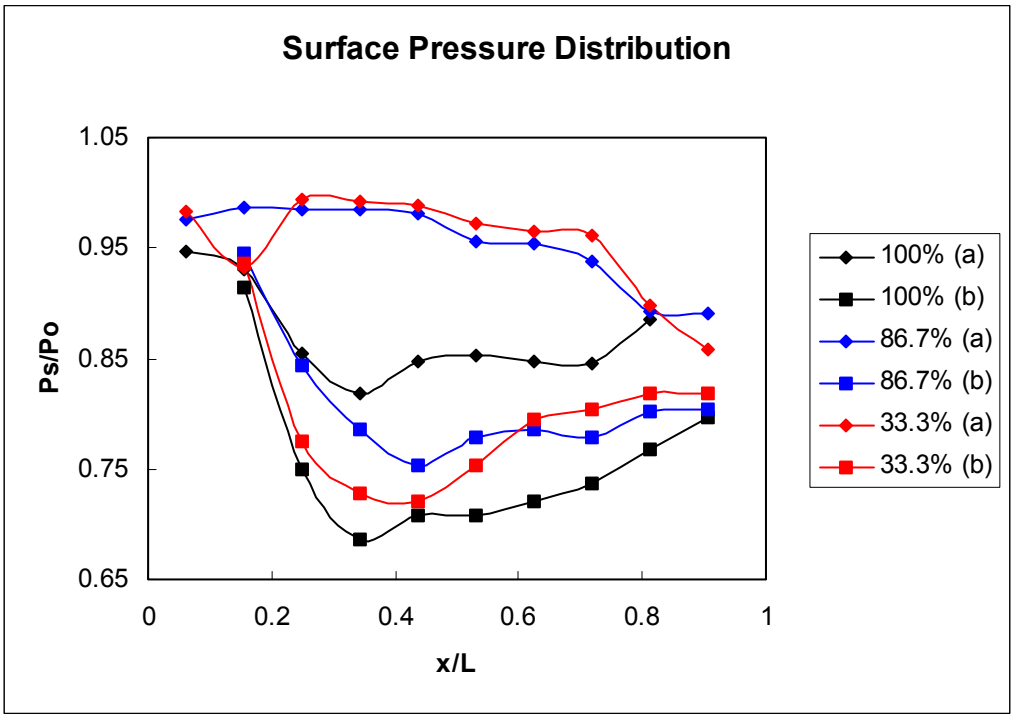


Figure 5.4: Surface pressure distributions on the test blade

The above figure shows the effects of tip leakage flow on surface pressure distribution. The data for 33.3% shows a large pressure gradient between the suction and pressure side. Leakage flow at the tip has not affected the pressure distribution around the blade surface. However, at 86.7% leakage flow has altered the pressure distribution

slightly. The data for 86.7% shows a smaller gradient compared to the 33.3% data. This indicates secondary flow over the blade surface in the direction of the blade tip. The 100% height, which is on the blade tip, has a much smaller pressure gradient than the 33.3% and 86.7% cases. The 100% height pressure gradient is greatly reduced because the clearance gap has induced secondary flow.

## 5.4 Flow Conditions

The test tunnel flow inlet conditions were measured using hot wire anemometry. The flow conditions are given in the following chart:

Table 5.5: Flow Conditions

| | |
|---|---|
| **Vi** | 135 |
| **Mi** | 0.4 |
| **Ve** | 298 |
| **Me** | 0.88 |
| **Pr** | 1.2 |
| **Re inlet** | 615000 |

The free stream turbulence intensity is measured with a single hot wire and a TSI and FA 100 data acquisition system. The turbulence intensity was, on average, Tu = 12.1% ± 1.6%.

## 5.5 Error Analysis

In order to determine the accuracy of this study, an error analysis is preformed using the methodology of Kline and McClintock (1953). The individual uncertainties are listed below:

$$\partial T_r = 3.341 \times 10^{-3} \tag{5-1}$$

$$\partial T_m = 3.372 \times 10^{-3} \tag{5-2}$$

$$\partial T_i = 0.027 \tag{5-3}$$

$$\partial t = 0.04 \tag{5-4}$$

$$\partial \alpha = 0.03 \tag{5-5}$$

$$\partial k = 0.03 \tag{5-6}$$

The average overall percent error is 6.4%. The maximum uncertainty will occur at regions close to the edges, and this uncertainty in measured 'h' can be close to ±12%.

# 6. Plain Tip Results: Effect of Gap Size

This chapter presents the results of heat transfer tests conducted on the plain tip geometry for two gap heights (1.0%, 2.6%). The results presented are the shroud pressure distributions, detailed tip heat transfer distributions, and camber line heat transfer line plots. The shroud pressure measurements are made 6.35 mm away from the suction side, 6.35 mm away from the pressure side, and along the camber line.

The following numbering system is used in all graphs: the plain tip blade with 1.0% gap height is referred to as Case 1, the plain tip blade with 2.6% gap height is referred to as Case 2. The shroud measurements for the suction side, pressure side, and camber line are referred to as a, b and c respectively as indicated in Table 6.1.

Table 6.1: Plain tip cases

| Plain Tip | | | |
|---|---|---|---|
| Case 1 | 1.0% gap | pressure side | Case 1a |
| | | suction side | Case 1b |
| | | camber line | Case 1c |
| Case 2 | 2.6% gap | pressure side | Case 2a |
| | | suction side | Case 2b |
| | | camber line | Case 2c |

## 6.1 Shroud Pressure Measurements

Figures 6.1 and 6.2 show the shroud measurements for Cases 1 and 2. Figure 6.1 relates the non-dimensional pressure (local static pressure divided by inlet total pressure: $P_s/P_o$) to non-dimensional length (position from leading edge to trailing edge divided by

the axial chord: x/Chord). The pressure ratio is highest at the blade leading edge were the flow stagnates.

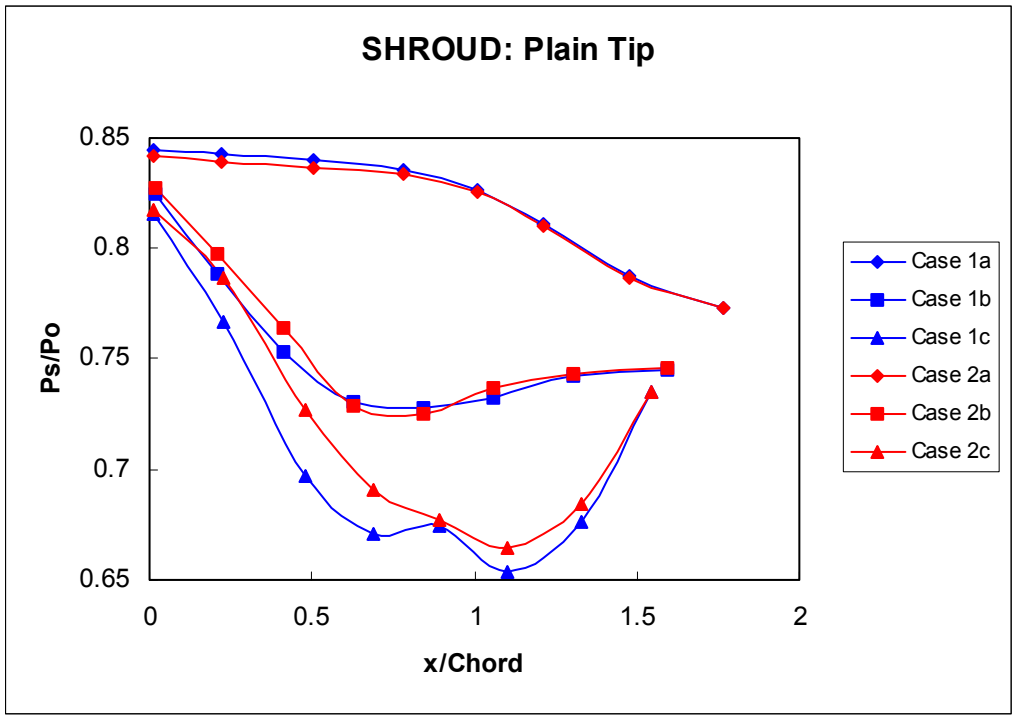


Figure 6.1: Plain tip shroud pressure distribution, line plot, 1.0, 2.6% gap

The air accelerates as it enters the clearance gap. This acceleration causes a drop in static pressure along the camber line. Then the flow expands while moving from the camber line to the suction side. This can be seen as the pressure recovery from the camber line to the suction side. Static pressure is lowest at the camber line. The levels of $P_s/P_o$ are similar for both tip gaps. However, the tip gap with 2.6% clearance has a larger area and hence allows more leakage flow for the same pressure gradient.

Figure 6.2 presents local shroud pressure results. The blade profile is

superimposed to show the local distributions. The results clearly show the effects of pressure drop along the camber line.

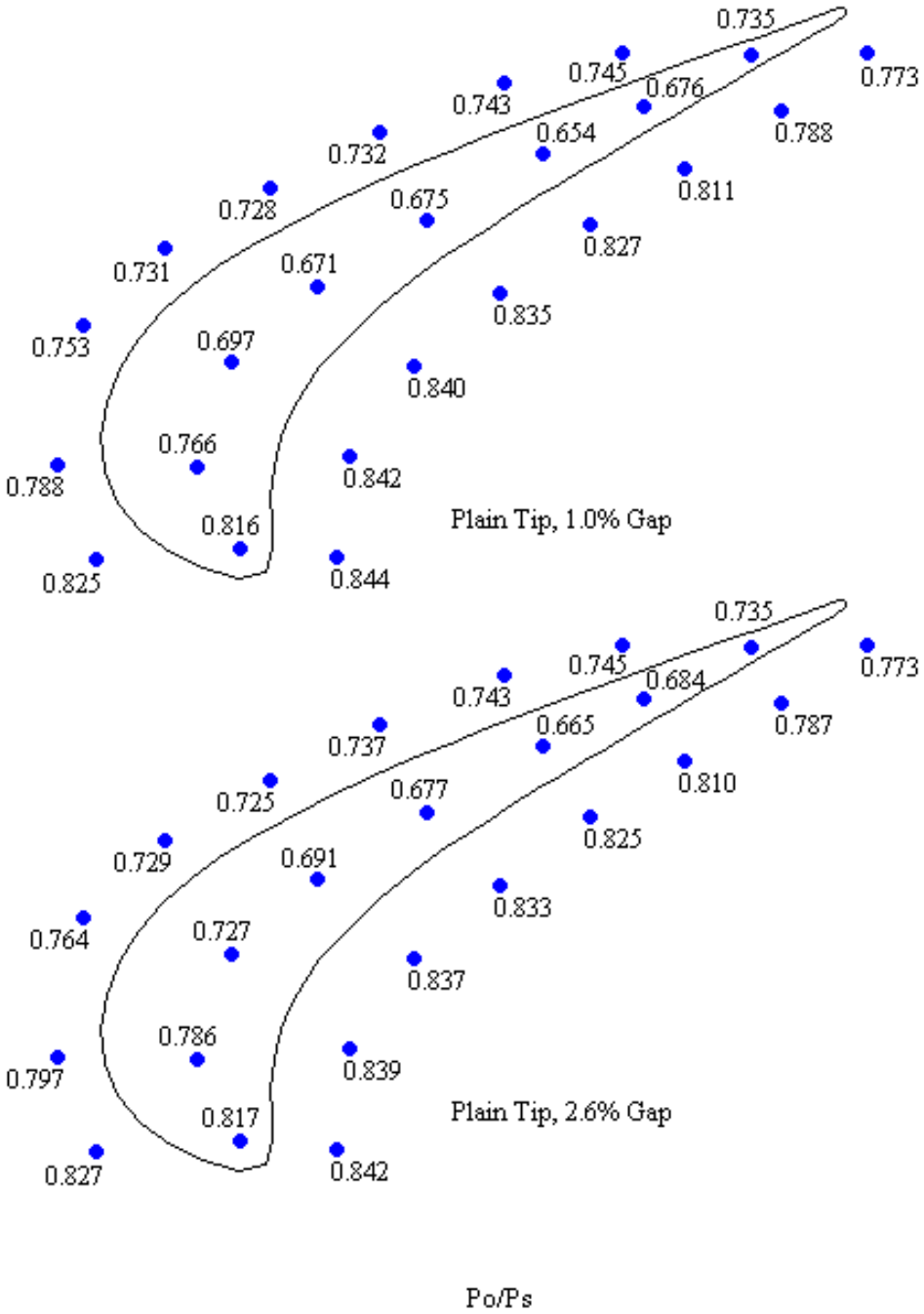


Figure 6.2: Plain tip shroud pressure distribution, 2-D plot, 1.0, 2.6% gap

## 6.2 Blade Tip Heat Transfer Coefficient Measurements: Color Plots

Figure 6.3 presents detailed tip heat transfer coefficients for the plain tip with 1.0% and 2.6% gap heights. A region of low heat transfer occurs at the middle of the blade for both Cases 1 and 2 due to the low pressure gradient across this area. This region, referred to as the "sweet spot", has values ranging from 470-640 $W/m^2 K$ for the 1% gap height and 555-640 $W/m^2 K$ for the 2.6% gap height. The sweet spot for Case 2 is smaller than that for Case1 due to reduced leakage flow.

Heat transfer coefficient values are subsequently higher along the trailing edge, close to pressure side. This area of high heat transfer is slightly removed from the pressure edge due to the fact that the blade model has a sharp edge; air separate from the tip edge and then reattaches on the tip surface. The heat transfer coefficient values in the trailing edge region range from 1500-2000 $W/m^2 K$ for both the 1% gap height and 2% gap height. Notice that the high heat transfer area is much larger for Case 2. As previously stated, a smaller gap height equates to reduced leakage flow over the plain tip, and this is why heat loads are smaller when the plain tip gap height is 1.0%. The clearance gap flow Reynolds number is larger for the larger gap thus enhancing heat load.

The following conclusion can be made about the gap flow field after looking at both the heat transfer and shroud pressure distributions. For a plain tip blade, regardless of gap height, the flow moves from high-pressure leading edge back, across the camber line to the low pressure points on the trailing edge suction side. The trend explains why heat transfer is low at the sweet spot and is high along the trailing edge. The importance of this observation will be expanded on in the Chapter 9, which discusses the effects of squealer depth on flow and heat transfer coefficients.

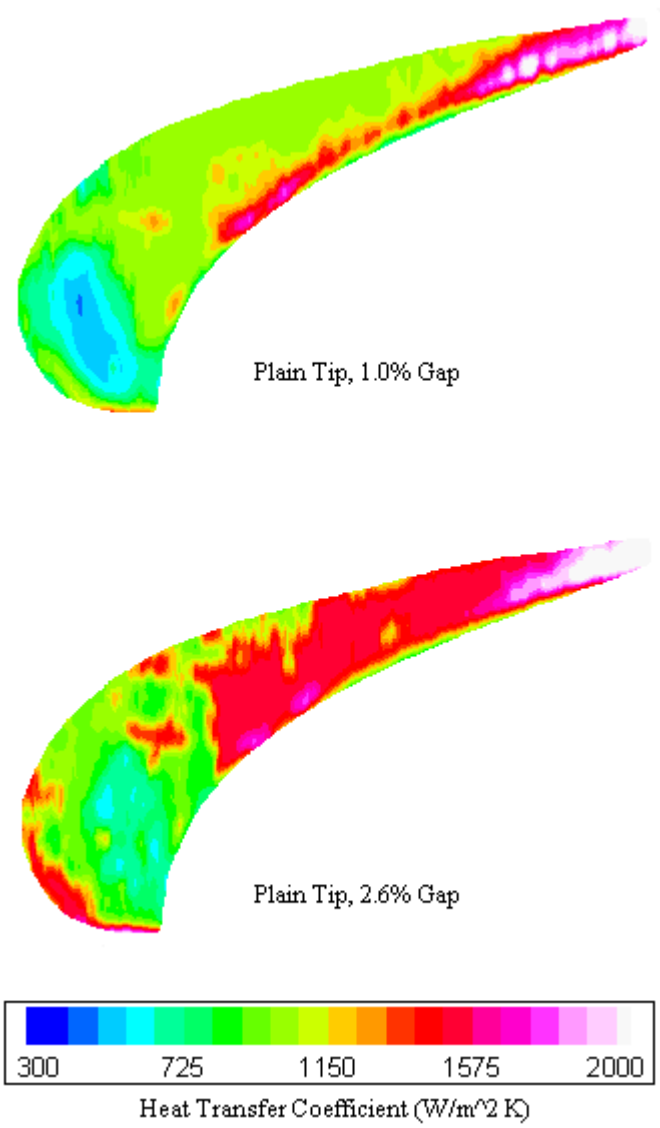


Figure 6.3: Plain tip heat transfer coefficient, 2-D color plot, 1.0, 2.6% gap

## 6.3 Blade Tip Heat Transfer Coefficient Measurements: Camber Line Plots

Figure 6.4 presents the camber line heat transfer coefficients from leading edge to trailing edge. The average heat transfer coefficient is higher along the camber line for the 2.6% gap height. There is a sharp spike right at the leading edge for both Cases 1 and 2; this ends at x/Chord = 0.1. Then the sweet spot is found for locations

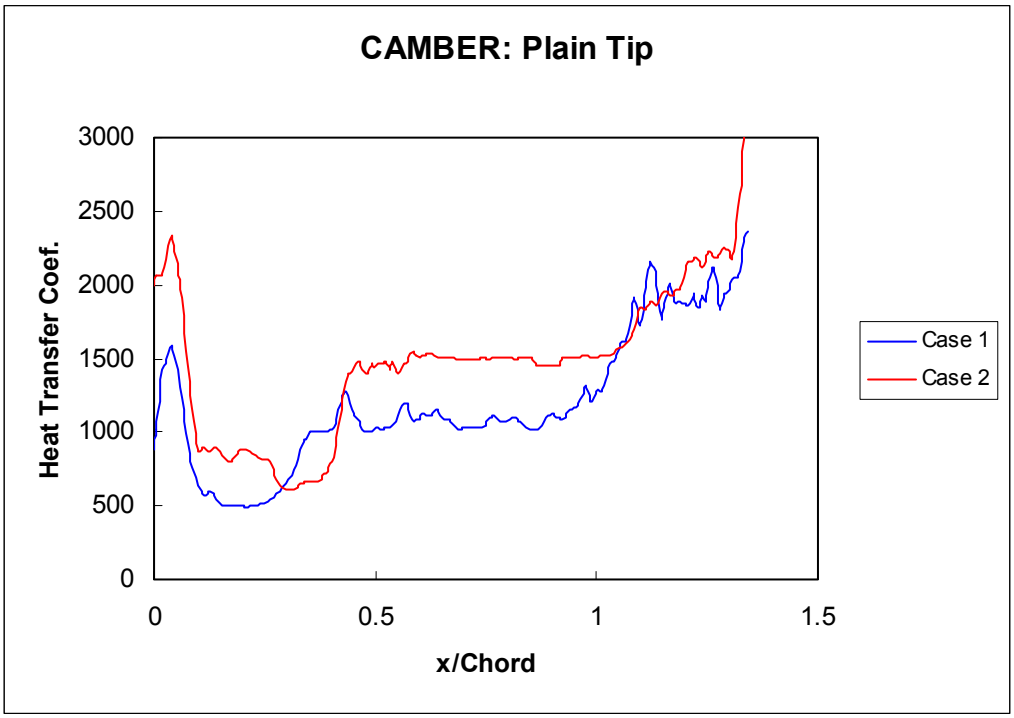


Figure 6.4: Plain tip heat transfer coefficient, camber line plot, 1.0, 2.6% gap

x/Chord = 0.1 – 0.4. The uniform values of 1000 and 1500 for Cases 1 and 2 respectively are seen up to x/Chord = 1.0. And then the coefficients rise toward the trailing edge. There is a distinct heat transfer gradient across the plain tip. Also the high heat transfer on the trailing edge is problematic in a real blade due to the fact that the thickness here is thin and eventually leads to degradation as shown in Figure 1.1.

# 7. Shallow Squealer Tip Results: Effect of Gap Size

This chapter presents the results of heat transfer tests on the shallow squealer tip geometry (D = 3.175 mm) for two gap heights (1.0%, 2.6%). As in Chapter 6, the results presented are shroud pressure distributions, detailed tip heat transfer distributions, and camber line heat transfer line plots. The shroud pressure measurements are made 6.35 mm away from the suction side, 6.35 mm away from the pressure side, and along the camber line.

The shallow squealer tip with 1.0% gap height is referred to as Case 3, and the shallow squealer tip with 2.6% gap height is referred to as Case 4. The shroud measurements for the suction side, pressure side, and camber line are referred to as a, b and c respectively as indicated in Table 7.1.

Figure 7.1: Shallow squealer cases

| Shallow Squealer | | | |
|---|---|---|---|
| Case 3 | 1.0% gap | pressure side | Case 3a |
| | | suction side | Case 3b |
| | | camber line | Case 3c |
| Case 4 | 2.6% gap | pressure side | Case 4a |
| | | suction side | Case 4b |
| | | camber line | Case 4c |

## 7.1 Shroud Pressure Measurements

Figures 7.1 and 7.2 show the shroud measurements for Cases 3 and 4. Figure 7.1 relates the non-dimensional pressure (local static pressure divided by upstream total pressure: $P_s/P_o$) to non-dimensional length (position from leading edge to trailing edge

divided by the axial chord: x/Chord). Like the plain tip data, pressure ratio is highest at the blade leading edge were the flow stagnates.

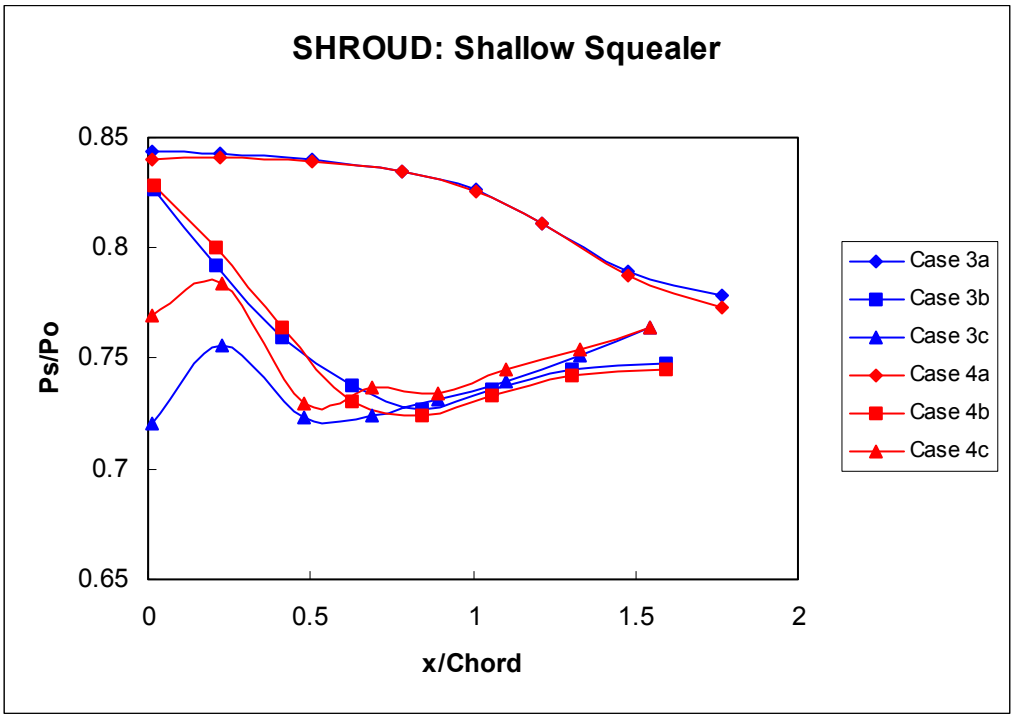


Figure 7.1: Shallow squealer shroud pressure distribution, line plot, 1.0, 2.6% gap

The air accelerates as it enters the clearance gap. Acceleration causes a drop in static pressure along the camber line. Then the flow expands while moving from the camber line to the suction side. Pressure is lowest at the camber line toward the leading edge. The levels of $P_s/P_o$ are similar for both tip gaps. Again, the tip gap with 2.6% clearance has a larger area and hence allows more leakage flow for the same pressure gradient.

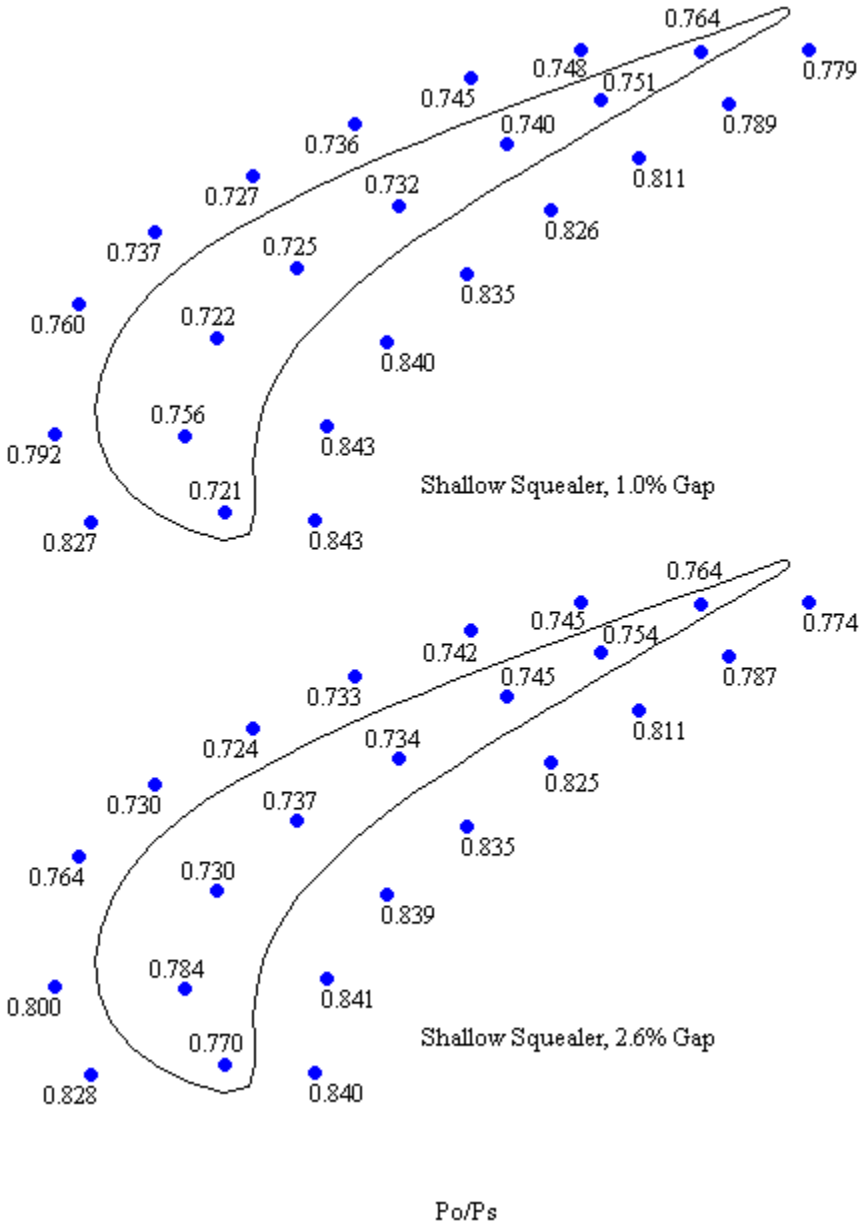


Figure 7.2: Shallow squealer shroud pressure distribution, 2-D plot, 1.0, 2.6% gap

Figure 7.2 presents local shroud pressure results. The blade profile is superimposed to show the local distributions. The results clearly show the effects of pressure drop of the camber line.

## 7.2 Blade Tip Heat Transfer Coefficient Measurements: Color Plots

Figure 7.3 presents detailed tip heat transfer coefficients for the shallow squealer tip with 1.0% and 2.6% gap heights. A region of high heat transfer at the middle of the blade for both Case 3 and 4 occurs due to the high pressure gradient across this area. This region, called the “hot spot”, has values ranging from 1065-1150 $W/m^2 K$ for the 1% gap height and 1320-1575 $W/m^2 K$ for the 2.6% gap height. The hot spot for Case 3 is smaller than that for Case 4.

Heat transfer coefficient values are reduced along the trailing edge. This is especially true close to pressure side. As air flows over the pressure side rim there is a large separation zone, this is the "line" of decreased heat transfer. Behind that line, air reaches the recess surface. The heat transfer coefficient values in the trailing edge region range from 640-895 $W/m^2 K$ for both the 1% gap height and 980-1065 $W/m^2 K$ 2.6% gap height. Notice that the high heat transfer area is much larger for Case 4. As was the case for the plain tip blade, a smaller gap height equates to reduced leakage flow over the squealer. The clearance gap flow Reynolds number is larger for the larger gap thus enhancing heat load.

The following conclusion can be made about the gap flow field after looking at both the heat transfer and shroud pressure distributions. For this shallow squealer blade tip, regardless of gap height, the flow moves from high-pressure leading edge back, across the leading edge portion of the camber line to the low pressure points on the leading edge suction side. A large amount of flow is sealed off from entering the trailing edge due to lack of any pressure gradient between the camber line and the suction side.

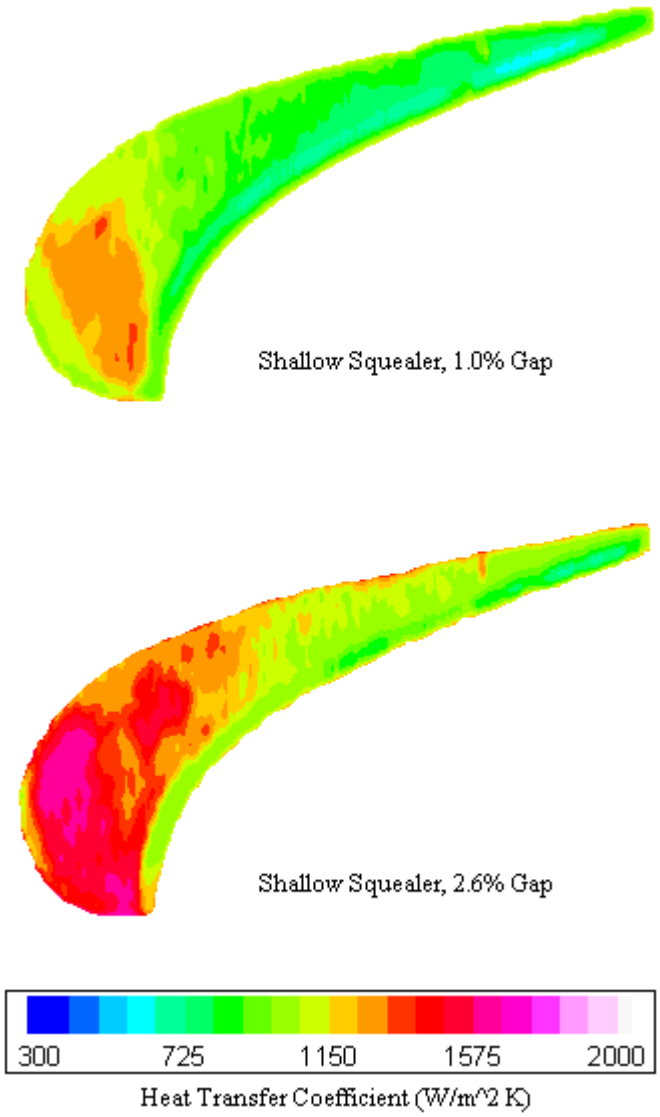


Figure 7.3: Shallow squealer heat transfer coeff., 2-D color plot, 1.0, 2.6% gap

## 7.3 Blade Tip Heat Transfer Coefficient Measurements: Camber Line Plots

Figure 7.4 presents the camber line heat transfer coefficients from leading edge to trailing edge. For the shallow squealer depth, the average heat transfer coefficient is higher along the camber line for the 2.6% gap height. The trend is similar for Cases 3

and 4 there is a downward slope from leading edge to trailing edge. And then the coefficients rise toward the trailing edge. Heat transfer gradient across the tip, with the exception of the hot spot, is relatively small.

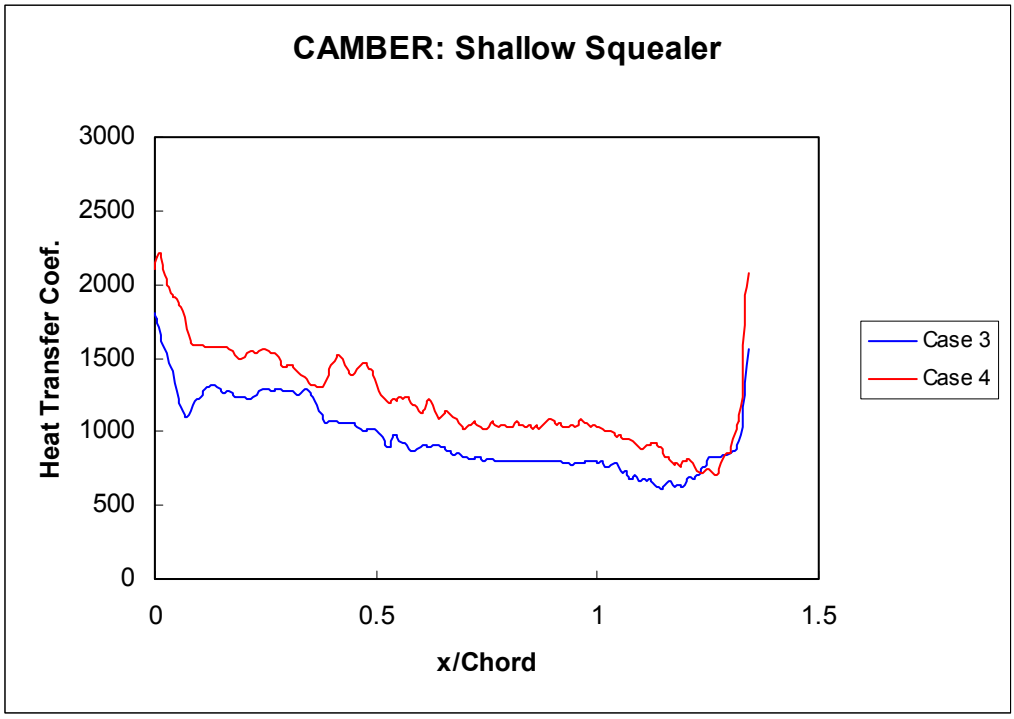


Figure 7.4: Shallow squealer heat transfer coefficient, camber line plot, 1.0, 2.6% gap

# 8. Deep Squealer Tip Results: Effect of Gap Size

This chapter presents the results of heat transfer tests on the shallow squealer tip geometry (D = 6.35 mm) for two gap heights (1.0%, 2.6%). As in the two previous chapters, the results presented are shroud pressure distributions, detailed tip heat transfer distributions, and camber line heat transfer line plots.

The shallow squealer tip with 1.0% gap height is referred to as Case 5, and the shallow squealer tip with 2.6% gap height is referred to as Case 6. The shroud measurements for the suction side, pressure side, and camber line are referred to as a, b and c respectively as indicated in Table 8.1.

Figure 8.1: Deep squealer cases

| Deep Squealer | | | |
|---|---|---|---|
| Case 5 | 1.0% gap | pressure side | Case 5a |
| | | suction side | Case 5b |
| | | camber line | Case 5c |
| Case 6 | 2.6% gap | pressure side | Case 6a |
| | | suction side | Case 6b |
| | | camber line | Case 6c |

## 8.1 Shroud Pressure Measurements

The shroud measurements for Cases 5 and 6 are presented in Figures 8.1 and 8.2. Figure 8.1 relates the non-dimensional pressure (local static pressure divided by upstream total pressure: $P_s/P_o$) to non-dimensional length (position from leading edge to trailing edge divided by the axial chord: x/Chord).

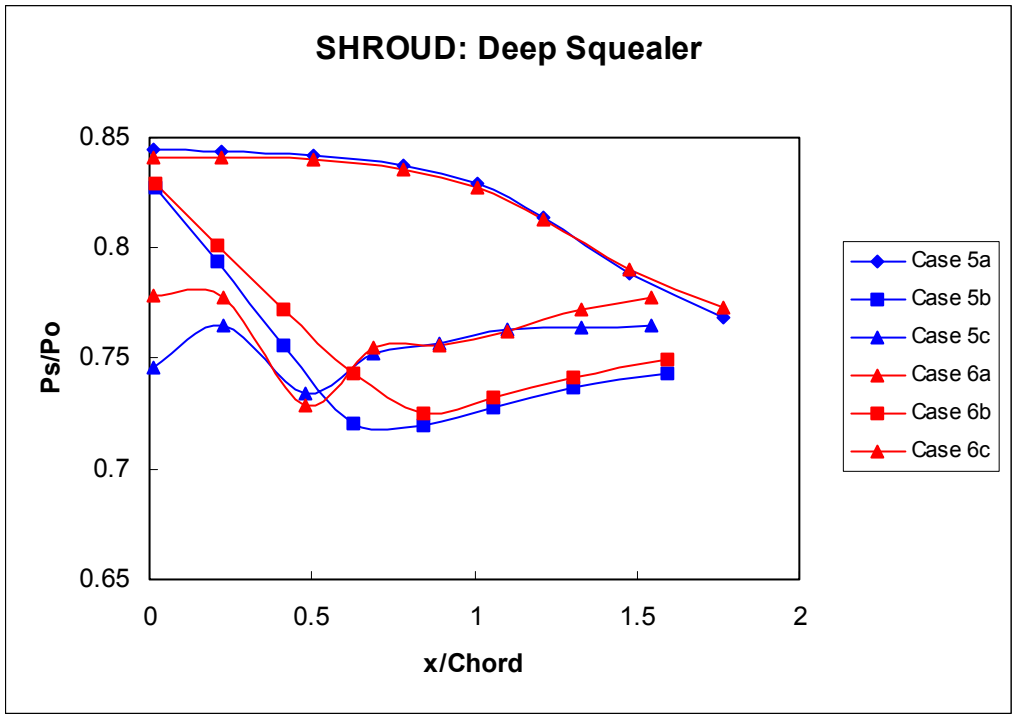


Figure 8.1: Deep squealer shroud pressure distribution, line plot, 1.0, 2.6% gap

The curves in Figure 8.1 resemble the curves for the shallow squealer case (Figure 7.1). As was the case with the shallow squealer, air accelerates into the clearance gap, causing a drop in static pressure at the camber line near the leading edge. The air decelerates as it moves from the camber line to the suction side. Static pressure is lowest at the camber line toward the leading edge. The level of $P_s/P_o$ are similar for both tip gaps, but the tip gap with 2.6% clearance has a larger area and hence allows more leakage flow for the same pressure gradient. In this case, however, the camber line pressure is higher than suction side along the trailing edge of the blade.

Figure 8.2 presents local shroud pressure results. The blade profile is superimposed to show the local distributions. The results clearly show the effects of pressure drop along the camber line.

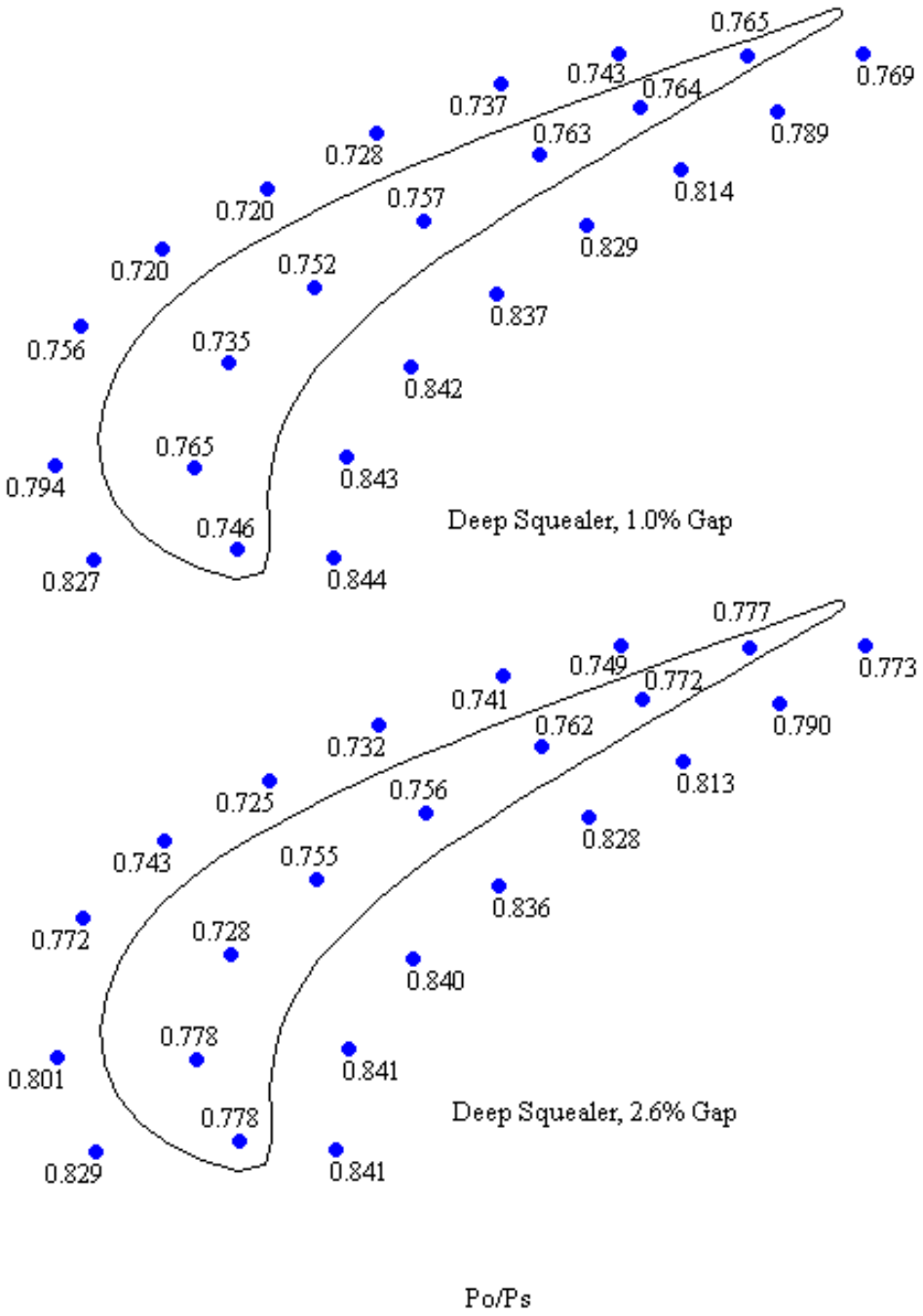


Figure 8.2: Deep squealer shroud pressure distribution, 2-D plot, 1.0, 2.6% gap

## 8.2 Blade Tip Heat Transfer Coefficient Measurements: Color Plots

Figure 8.3 presents detailed tip heat transfer coefficients for the deep squealer tip with 1.0% and 2.6% gap heights. The hot spot has values ranging from 980-1065 W/m$^2$

K for the 1% gap height and 1320-1490 W/m$^2$ K for the 2.6% gap height. The hot spot for Case 5 is smaller than that for Case 6.

Heat transfer coefficient values are low along the trailing edge. A thin line of extremely low heat coefficient value extends along the pressure side from the trailing edge up to the blade midpoint. This line is much longer for the 1.0% gap, due to the fact that air flow is more restricted. The explanation for the line is that behind the pressure side rim there is a large separation zone. Behind that line, air reattaches on the recess surface. The heat transfer coefficient values in the trailing edge region range from 385-810 W/m$^2$ K for both the 1.0% gap height and 385-980 W/m$^2$ K for the 2.6% gap height. Notice that the high heat transfer area is much larger for Case 6. As was the case for the two previous blade tip configurations, a smaller gap height equates to reduced leakage flow over the squealer, and the clearance gap flow Reynolds number is larger for the larger gap thus enhancing heat load.

## 8.3 Blade Tip Heat Transfer Coefficient Measurements: Camber Line Plots

Figure 8.4 presents the camber line heat transfer coefficients from leading edge to trailing edge. For this squealer depth, the average heat transfer coefficient is higher along the camber line for the 2.6% gap height. The trend is similar for Cases 5 and 6 there is a downward slope from leading edge to trailing edge. And then the heat transfer coefficients rise toward the trailing edge. Heat transfer gradient across the tip, with the exception of the hot spot, is relatively small.

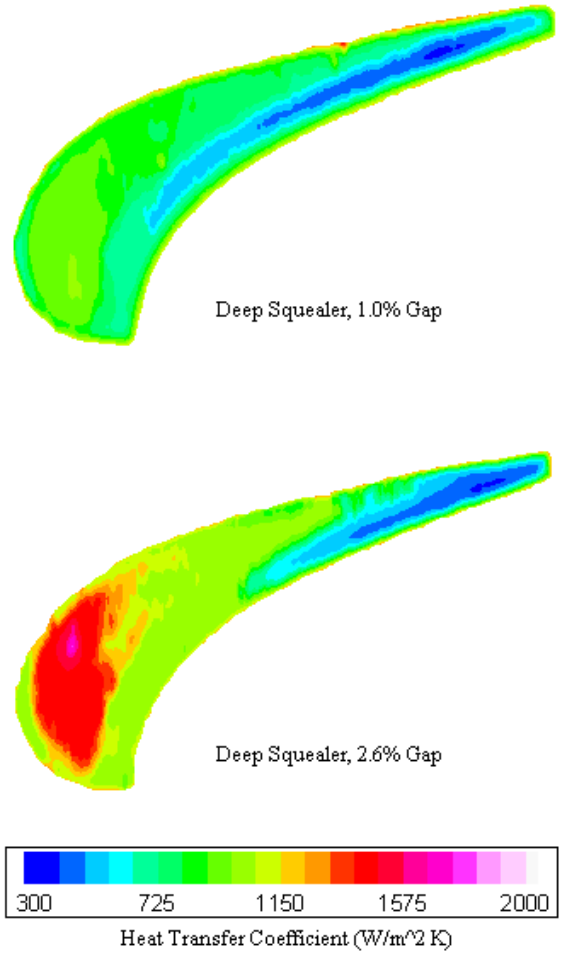


Figure 8.3: Deep squealer heat transfer coefficient, 2-D color plot, 1.0, 2.6% gap

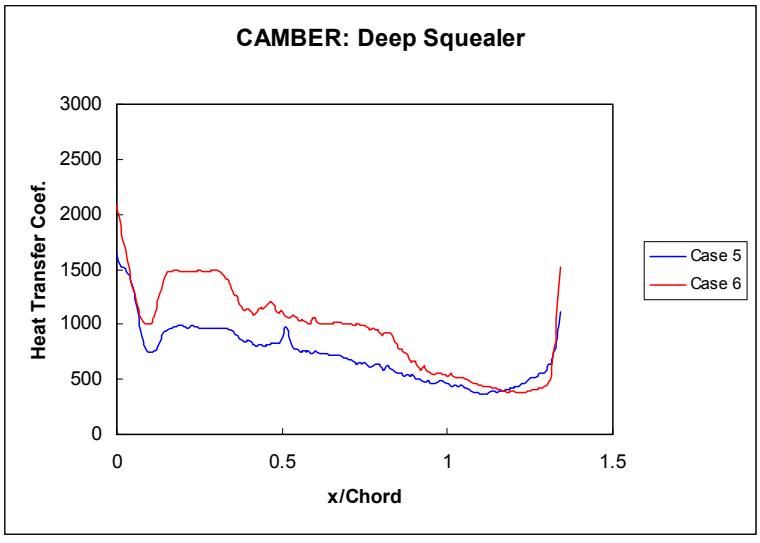


Figure 8.4: Deep squealer heat transfer coefficient: camber line plot, 1.0, 2.6% gap

# 9. Plain Tip vs. Shallow and Deep Squealers

Chapters 6, 7, and 8 presented and discussed the effects of gap height on a plain tip, shallow squealer (D = 3.175 mm), and deep squealer (D = 6.35 mm). This chapter presents and discusses the differences in heat transfer coefficient and flow between the three tip geometries.

Table 9.1: Cases

| Cases | | |
|---|---|---|
| **Plain Tip** | Case 1 | 1.0% gap |
| | Case 2 | 2.6% gap |
| **Shallow Squealer** | Case 3 | 1.0% gap |
| | Case 4 | 2.6% gap |
| **Deep Squealer** | Case 5 | 1.0% gap |
| | Case 6 | 2.6% gap |

| Symbols | |
|---|---|
| pressure side | a |
| suction side | b |
| camber line | c |

## 9.1 Shroud Pressure Measurements

Figures 9.1 and 9.2 present the shroud data in a manner conducive to comparing the different tip geometries. It is clear, when looking at the pressure side curves, that flow is unaffected by tip configuration until it passes the pressure rim. However, the pressure distributions along the camber line are dependent on tip geometry. The largest pressure gradient for the squealer tip is toward the leading edge. This means the flow travels over the front of the blade. In contrast, the plain tip has a large pressure gradient from leading edge to the back of the suction side. This is the path followed by the leakage flow. Figure 9.3 shows these flow trends.

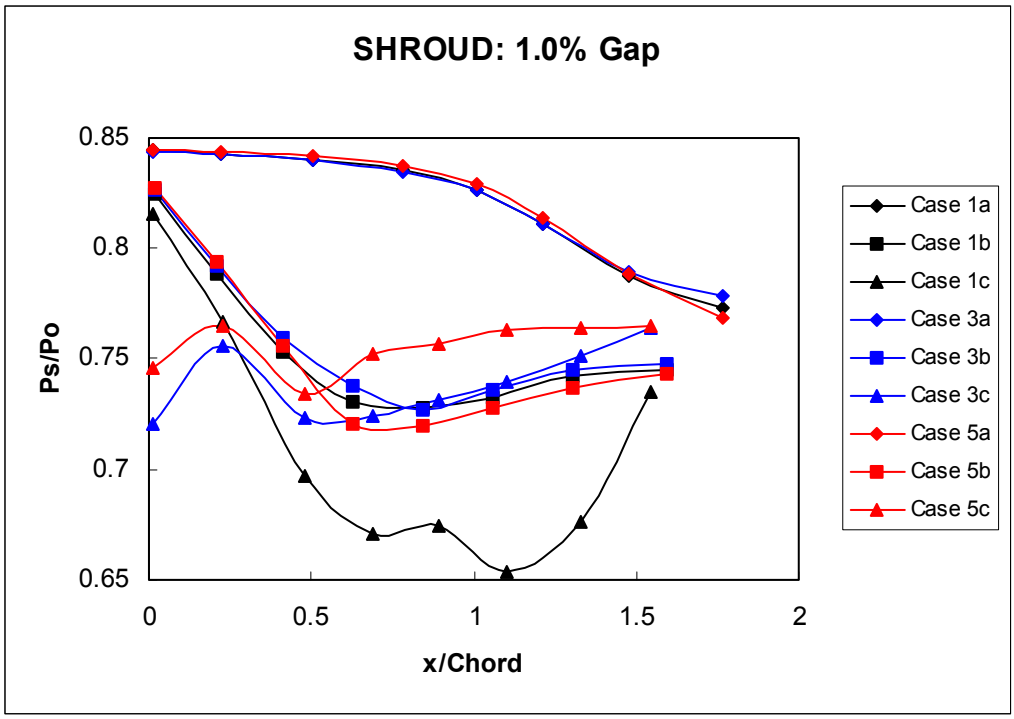


Figure 9.1: 1.0% gap shroud pressure, plain tip, shallow squealer, deep squealer

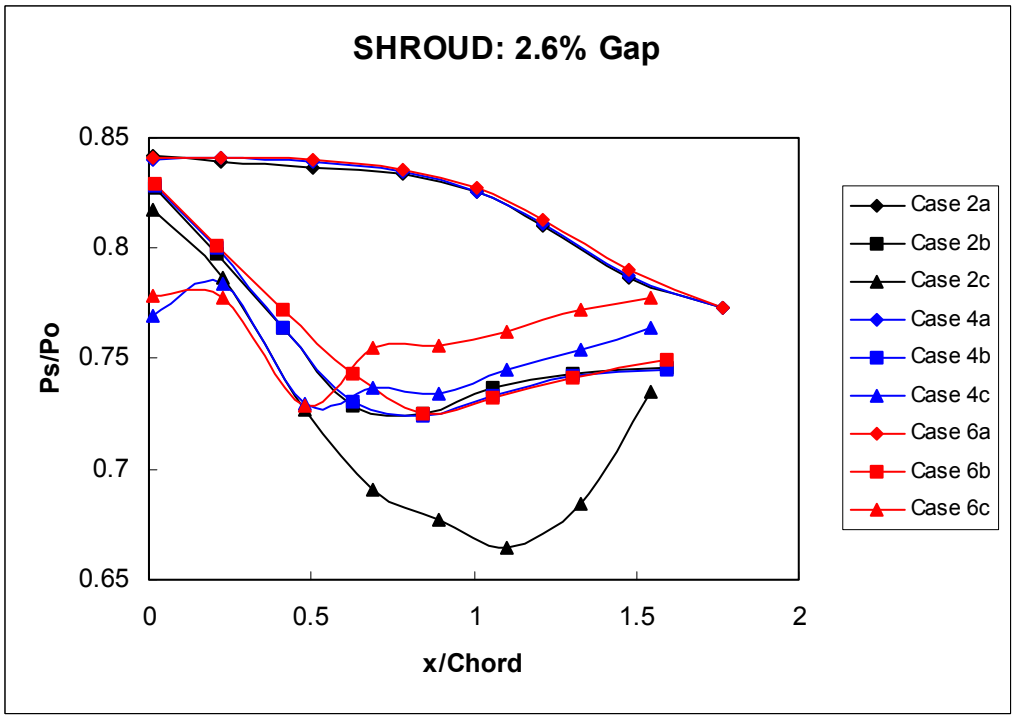


Figure 9.2: 2.6% gap shroud pressure, plain tip, shallow squealer, deep squealer

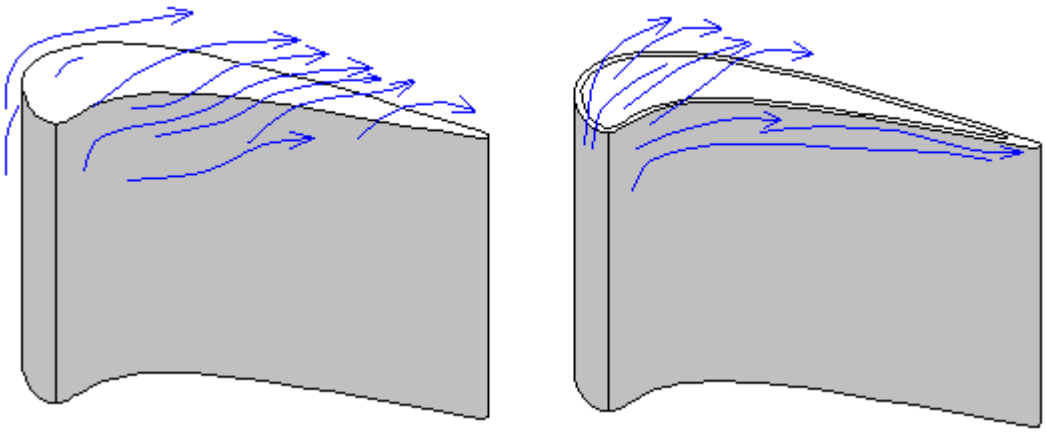

Figure 9.3: Plain tip and squealer flow

## 9.2 Blade Tip Heat Transfer Coefficient Measurements: Color Plots

The heat transfer data supports the comments made in the previous chapter about flow paths over the blade tip. The plain tip blades in Figures 9.4 and 9.5 have a sweet spot at the leading edge and high heat transfer coefficients over the trailing edge. This is caused by the flow pattern: air moves over the back end of the tip. The squealer tip has a different flow pattern that causes a reverse trend compared to the plain tip. As mentioned in the previous section, air flow from the leading edge to the suction side midpoint. The reversed trend in heat loading is beneficial because it means the thinner part of the blade is better protected.

While the flow pattern over the deep squealer and shallow squealer is the same, there is a difference in heat load values. Figures 9.4 and 9.5 obviously show that the deep squealer has, on average, lower values of heat transfer. This means that a deep squealer will better restrict leakage flow. Heat transfer coefficients for the deep squealer are also significantly lower than values on the plain tip blade.

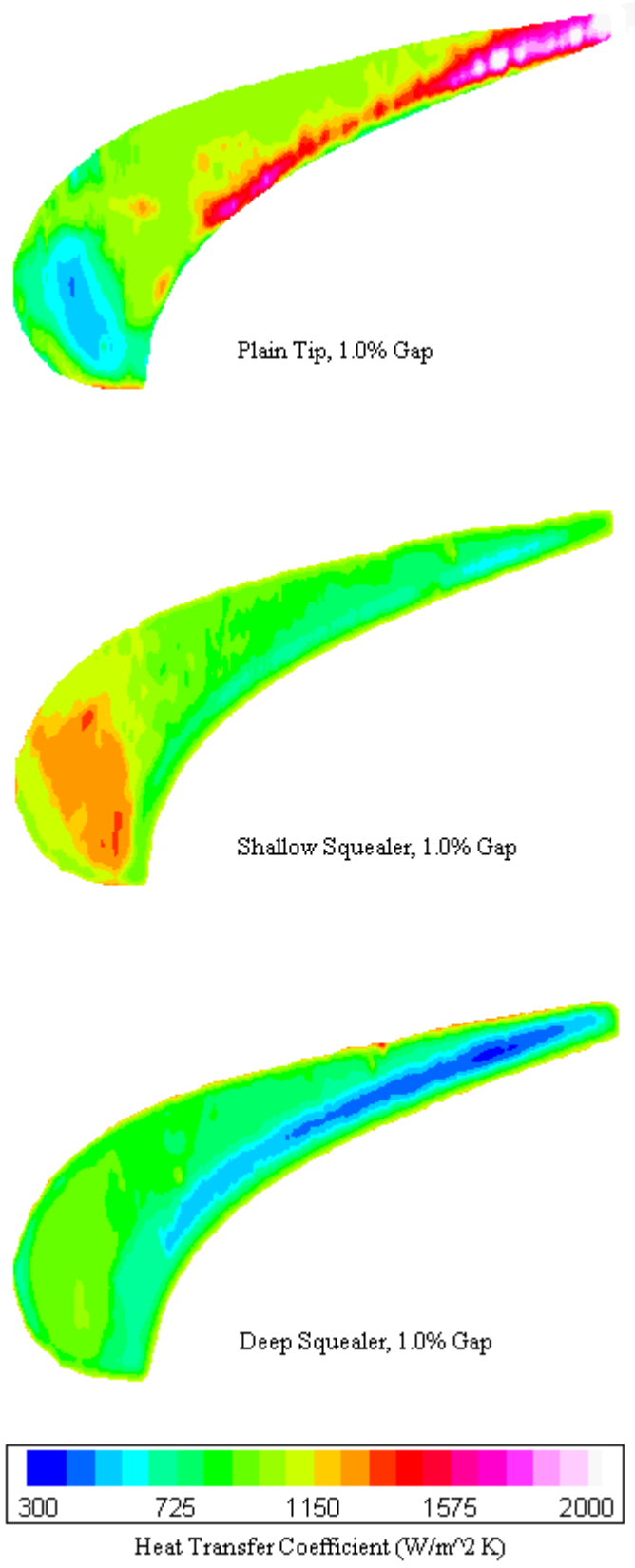


Figure 9.4: 1.0% gap heat transfer coeff., 2-D color plot, plain tip, shallow, deep squealer

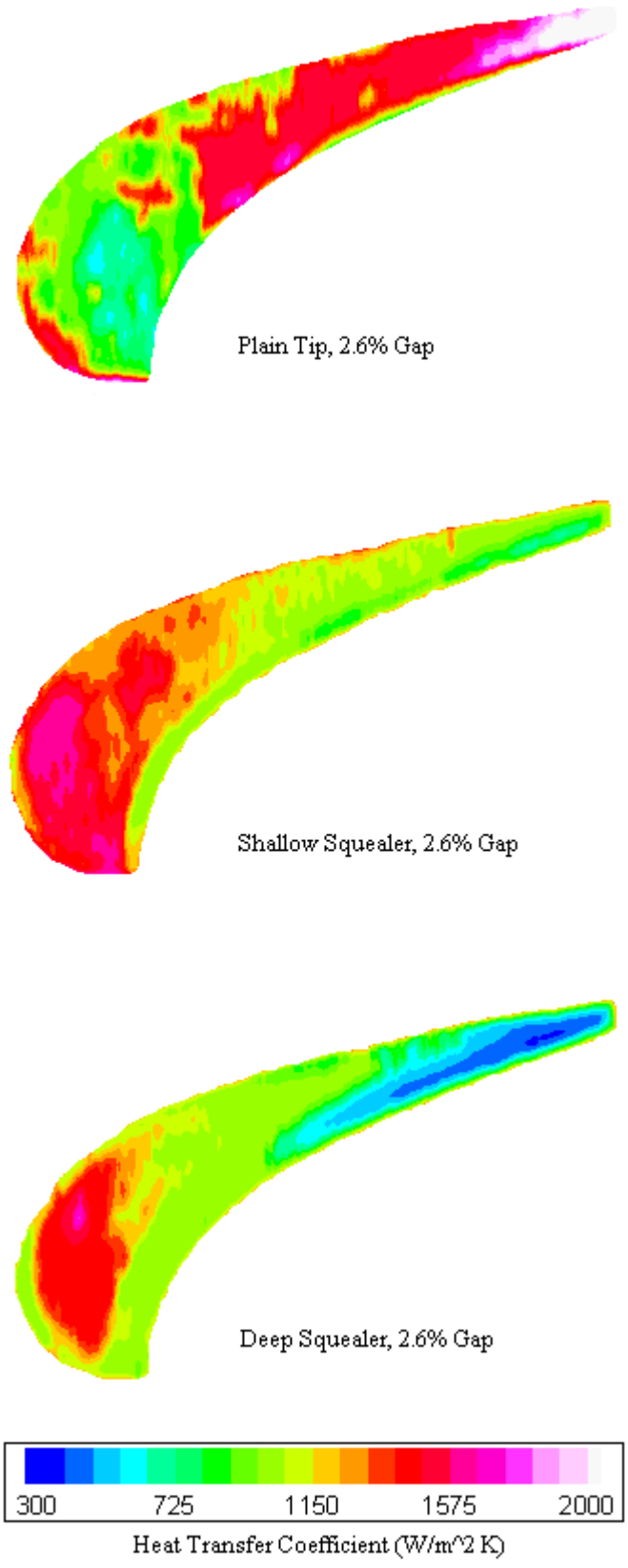


Figure 9.5: 2.6% gap heat transfer coeff., 2-D color plot, plain tip, shallow, deep squealer

## 9.3 Blade Tip Heat Transfer Coefficient Measurements: Camber Line Plots

Figures 9.6 and 9.7 show the camber line data. Obviously the deep squealer has lowest heat transfer values. The squealers have lower heat loads, in general, and a smaller slop. The trailing edge heat transfer coefficients are much lower for both squealers when compared to the plain tip blade. Lower heat transfer on the trailing edge is beneficial because the trailing edge is thinner than the leading edge. The thinner trailing edge is more susceptible to damage than the robust leading edge.

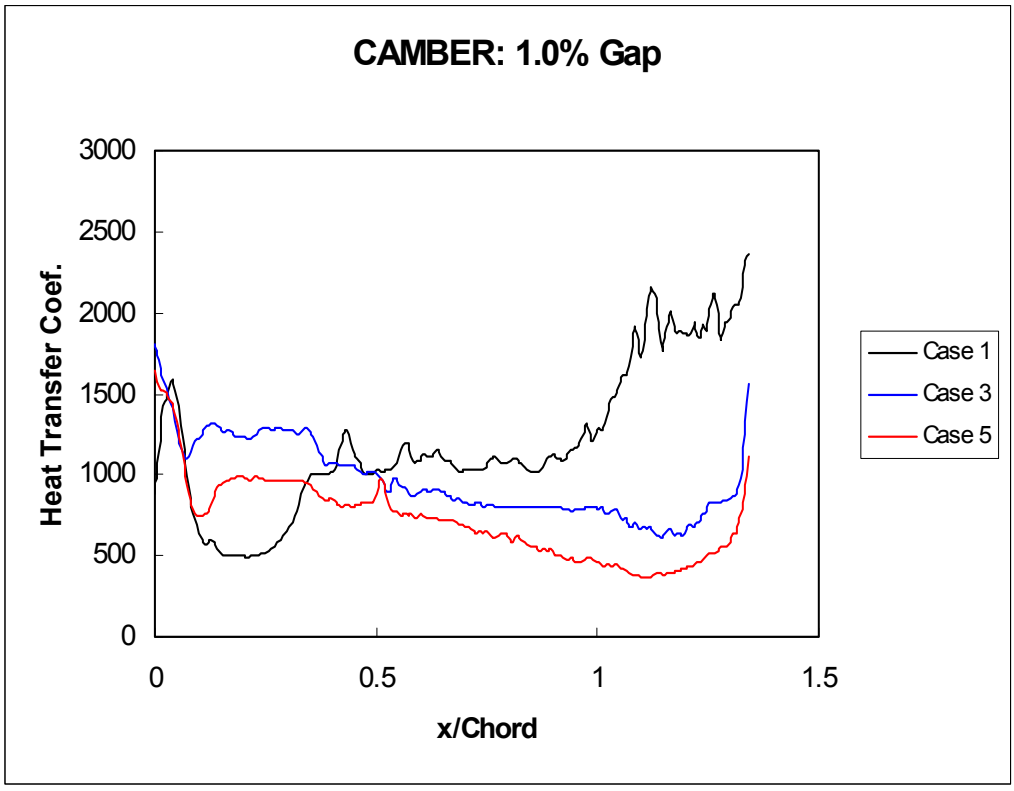


Figure 9.6: 1.0% gap h.t. coeff., camber line plots, plain tip, shallow, deep squealer

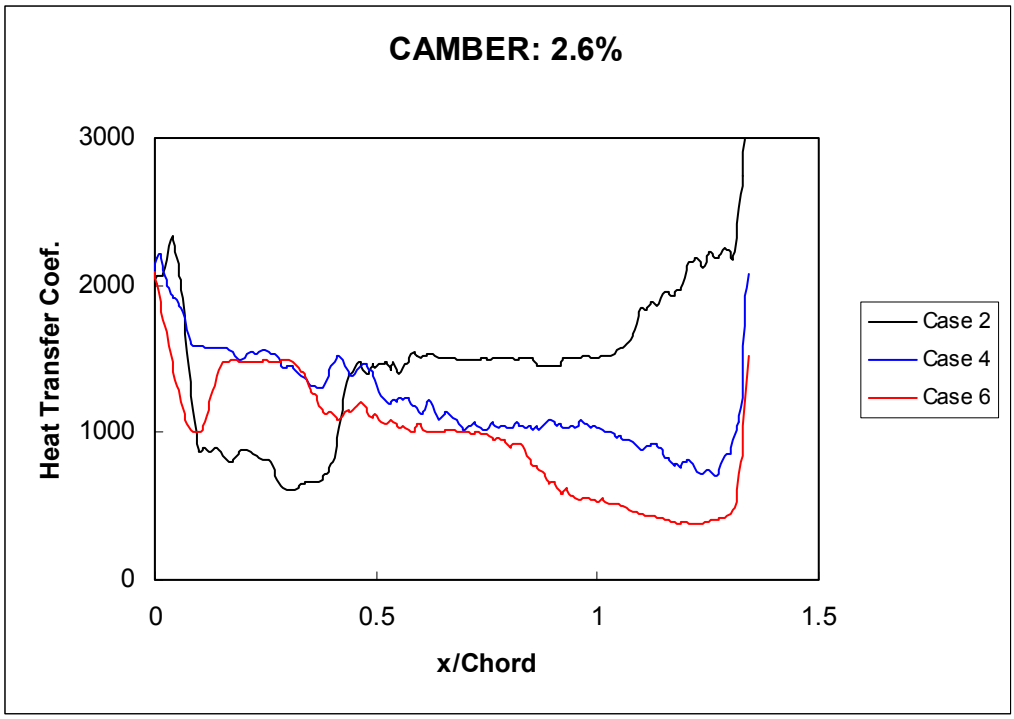

Figure 9.7: 2.6% gap h.t. coeff., camber line plots, plain tip, shallow, deep squealer

# 10. Conclusions

- A blow-down test was preformed to determine the heat transfer coefficients on the tip of a high pressure turbine blade with a plain tip and two squealer depths (D = 6.35, 3.175 mm) with two gap heights, 1.0, 2.6%
- Flow over the plain tip blade moves from the leading edge pressure side to the trailing edge suction side
- Flow over the squealer tip blades moves from the leading edge pressure side to the midpoint of the suction side
- The deepest squealer, D = 6.35 mm, reduced leakage flow over the blade tip more than the other tested geometries
- The deepest squealer, D = 6.35 mm, reduced heat transfer the blade tip more than the other tested geometries
- The small gap height, 1.0%, reduced leakage flow over the blade tip more the larger 2.6% gap height
- The small gap height, 1.0%, reduced heat transfer to the blade tip more the larger 2.6% gap height

Future recommendations are made for film cooling studies. The results clearly show that the pressure side film holes will provide effective film cooling for the plain tip. Tip holes near the leading edge will be beneficial by supplying coolant for the squealer tips.

# References


Ameri, A.A., Bunker, R.S., 1999, "Heat Transfer and Flow on th First Stage Blade Tip of a Power Generation Gas Turbine Part 2: Simulation Results," *ASME Journal of Turbomachinery*, Vol. 122, pp. 272-277.

Azad, G.S., Han, J.C., Boyle, R.J., "Heat Transfer and Flow on the Squealer Tip of a Gas Turbine Blade," Proceeding of: *International Gas Turbine and Aeroengine Congress and Exposition*, Munich, Germany, May 2000, 2000-GT-195

Azad, G.S., Han, J.C., Bunker, R.S., Lee, C.P., "Effect of Squealer Geometry Arrangement on Gas Turbine Blade Tip Heat Transfer," Proceeding of: *International Mechanical Engineering Congress and Exposition*, New York, New York, November 2001, IMECE2001/HTD-24314

Bunker, R.S., Bailey, J.C., 2001, "Effect of Squealer Cavity Depth and Oxidation on Turbine Blade Tip Heat Transfer," *International Gas Turbine and Aeroengine Congress and Exposition*, New Orleans, June 2001

Bunker, R.S., Bailey, J.C., 2000, "An Experimental Study of Heat Transfer and Flow on a Gas Turbine Blade Tip With Various Tip Leakage Sealing Methods," Proceedings of the 4th HMT/ASME Heat and Mass Transfer Conference, Paper No. HMT2000-055, pp. 411-416

Bunker, R.S., Bailey, J.C., Ameri, A.A., 1999, "Heat Transfer and Flow on the First Stage Blade Tip of a Power Generation Gas Turbine: Part 2-Experimental Results," *ASME Journal of Turbomachinery*, Vol. 122, pp. 263-271

Bindon, J.P., 1989, "The Measurement and Formation of Tip Clearance Loss" *ASME Journal of Turbomachinery*, Vol. 111, pp. 257-263

Mayle, R.E., Metzger, D.E., "Heat Transfer at the Tip of an Unshrouded Turbine Blade" Proceedings of the 7th International Heat Transfer Conference, Vol. 3, pp. 87-92

Metzger, D.E., Bunker, R.S., Chyu, M.K., 1989, "Cavity Heat Transfer on a Transverse Grooved Wall in a Narrow Flow Channel," *ASME Journal of Heat Transfer*, Vol. 111, pp. 73-79

Metzger, D.E., Dunn, M.G., Hah, C., "Turbine Tip and Shroud Heat Transfer," Proceeding of: *International Gas Turbine and Aeroengine Congress and Exposition*, Brussels, Belgium, September 1990, 90-GT-333

Metzger, D.E., Rued, K., "The Influence of Turbine Clearance Gap Leakage on Passage Velocity and Heat Transfer Near Blade Tips Part 1: Sink Flow Effects on Blade Pressure Side," Proceeding of: *International Gas Turbine and Aeroengine Congress and Exposition*, Amsterdam, Netherlands, June 1988, 88-GT-98

Moore J., Moore J.G., Henry, G.S., Chaudhry, U., 1989, "Flow and Heat Transfer in Turbine Tip Gaps," *ASME Journal of Turbomachinery*, Vol. 111, pp. 300-309

Rued, K., Metzger, D.E., "The Influence of Turbine Clearance Gap Leakage on Passage Velocity and Heat Transfer Near Blade Tips Part 2: Source Flow Effects on Blade Suction Side," Proceeding of: *International Gas Turbine and Aeroengine Congress and Exposition*, Amsterdam, Netherlands, June 1988, 88-GT-99

Yamamoto, A., 1989, "Endwall Flow/Loss Mechanisms in a Linear Turbine Cascade With Blade Tip Clearance," *ASME Journal of Turbomachinery*, Vol. 111, pp. 264-275

Yang, T.T., Diller, T.E., "Heat Transfer and Flow for a Grooved Turbine Blade Tip in a Transonic Cascade," Proceeding of: *International Mechanical Engineering Congress and Exposition*, San Francisco, ASME No. 95-WA/HT-29

Yaras, M., Yingkang, Z., Sjolander, S.A., 1989, "Flow Field in the Tip Gap of a Planar Cascade of Turbine Blades," *ASME Journal of Turbomachinery*, Vol. 111, pp. 276-283

# Vita

David Michael Kontrovitz was born on June 28th, 1977, in Princeton, New Jersey. He received the degree of Bachelor of Science in Mechanical Engineering in 2000 from Louisiana State University. He joined the Louisiana State University Mechanical Engineering graduate program in Fall 2000. He is a candidate for the degree of Master of Science in Mechanical Engineering in August 2002. He will join Pratt & Whitney in July as a Staff Engineer.